European Journal of Medicinal Chemistry 221 (2021) 113480

Contents lists available at ScienceDirect

European Journal of Medicinal Chemistry

journal homepage: http://www.elsevier.com/locate/ejmech

Design, synthesis and evaluation of novel 9-arylalkyl-10-methylacridinium derivatives as highly potent FtsZ-targeting antibacterial agents

Di Song, Nan Zhang, Panpan Zhang, Na Zhang, Weijin Chen, Long Zhang, Ting Guo, Xiaotong Gu, Shutao Ma*

Department of Medicinal Chemistry, Key Laboratory of Chemical Biology (Ministry of Education), School of Pharmaceutical Sciences, Cheeloo College of Medicine, Shandong University, 44 West Wenhua Road, Jinan, 250012, China

ARTICLE INFO

Article history:
Received 26 March 2021
Received in revised form
13 April 2021
Accepted 15 April 2021
Available online 28 April 2021

Keywords:
9-Arylalkyl-10-methylacridinium derivatives
Design and synthesis
Antibacterial activity
FtsZ inhibitor
Structure-activity relationships

ABSTRACT

With the increasing incidence of antibiotic resistance, new antibacterial agents having novel mechanisms of action hence are in an urgent need to combat infectious diseases caused by multidrug-resistant (MDR) pathogens. Four novel series of substituted 9-arylalkyl-10-methylacridinium derivatives as FtsZ inhibitors were designed, synthesized and evaluated for their antibacterial activities against various Gram-positive and Gram-negative bacteria. The results demonstrated that they exhibited broad-spectrum activities with substantial efficacy against MRSA and VRE, which were superior or comparable to the berberine, sanguinarine, linezolid, ciprofloxacin and vancomycin. In particular, the most promising compound **15f** showed rapid bactericidal properties, which avoid the emergence of drug resistance. However, **15f** showed no inhibitory effect on Gram-negative bacteria but biofilm formation study gave possible answers. Further target identification and mechanistic studies revealed that **15f** functioned as an effective FtsZ inhibitor to alter the dynamics of FtsZ self-polymerization, which resulted in termination of the cell division and caused cell death. Further cytotoxicity and animal studies demonstrated that **15f** not only displayed efficacy in a murine model of bacteremia *in vivo*, but also no significant hemolysis to mammalian cells. Overall, this compound with novel skeleton could serve as an antibacterial lead of FtsZ inhibitor for further evaluation of drug-likeness.

1. Introduction

Infections caused by bacteria have long been common diseases that even severely threaten human's life. Thanks to the discovery of penicillin in 1928, and the subsequent application of various antibacterial drugs, millions of lives have been saved. However, the use of antibacterial drugs inevitably leads to the emergence of bacterial resistance, and in recent years, especially, the widespread use or even abuse of antibacterial drugs greatly has accelerated the prevalence of bacterial resistance, which are undoubtedly exacerbating the threat of clinical infections [1]. For example, the appearance of methicillin-resistant *Staphylococcus aureus* (MRSA) and vancomycin-resistant *Enterococcus* (VRE) contributes to the enormous difficulty in fighting against bacterial infections [2,3]. Thus, the discovery of new antibacterial targets and development of effective antibacterial drugs with new mechanism should be accelerated to cope with this issue [4].

The bacterial cell division machinery involves many essential proteins that are extremely sensitive to perturbation by small molecules [5]. As a eukaryotic tubulin analogue, the filamentous temperature-sensitive protein Z (FtsZ) is a key protein involved in bacterial cell division [6,7]. When bacterial cells divide, FtsZ polymerizes into tubulin-like protofilaments at mid-cell that serves as a highly dynamic cytoskeleton scaffold for the recruitment and organization of other cell division proteins in the presence of guanosine triphosphate (GTP) to complete the bacterial cell division [8]. The arrangement of protofilaments is head to tail, which is followed to assemble into bundles at the site of septum formation. Intervention of this normal biological function will result in the inhibition of bacterial division and eventually the death of bacteria [9]. In addition, FtsZ is highly conservative in the bacterial kingdom and plays an essential role in prokaryotic cell division. Therefore,

* Corresponding author.
E-mail address: mashutao@sdu.edu.cn (S. Ma).

https://doi.org/10.1016/j.ejmech.2021.113480
0223-5234/

FtsZ has been a promising new target for the development of new antibacterial drugs. At present, many FtsZ inhibitors have been reported to exhibit potent antibacterial activity. A few representative natural and synthesized molecules are shown in Fig. 1 [10–15].

Sanguinarine and berberine with a quaternary pyridinium core, which are two alkaloids extracted from natural products, have been identified as FtsZ inhibitors that can alter the Z-ring formation and disturb the function of FtsZ protein [16,17]. For example, sanguinarine can inhibit the growth of *Escherichia. coli* and *Bacillus subtilis* by inhibiting Z-ring formation without affecting nucleoid segregation. Its IC_{50} values for *E. coli* and *B. subtilis* are 4.6 ± 0.8 μg/mL and 1.0 ± 0.3 μg/mL, respectively. However, sanguinarine may depolymerize microtubules and produce harmful side effects in mammals, which is a potential drawback in the development of sanguinarine as antibacterial drug [18]. Berberine, an alkaloid with similar structure to sanguinarine, can inhibit GTPase activity and reduce FtsZ polymerization. Although berberine has no inhibitory effect on microtubules, its antibacterial activity is poor against Gram-positive bacteria with the minimum inhibitory concentration values (MICs) in the range of 100–400 μg/mL [19]. Recent literatures have reported that some compounds possessing the quaternary or binary pyridinium scaffold with aromatic hydrophobic groups can significantly enhance antibacterial activity via targeting FtsZ [20–24]. Our group has been committed to investigating new FtsZ inhibitors through structural simplification of natural products such as sanguinarine and berberine, etc. We reported a series of 5-methyl phenanthridium compounds with moderate activity against a broad range of Gram-positive bacteria and none of the compounds enhanced polymerization of mammalian tubulin even though they were at higher concentrations than the positive control paclitaxel [25]. Further, we accomplished the synthesis of novel 5-methyl-2-phenyl phenanthridium derivatives with an unexpected increase in antibacterial activity [26]. Docking results demonstrated the phenanthridium compound combined in a relatively narrow cleft delimited by the H7-helix, the T7-loop and C-terminal subdomain. We found benzodioxolane of sanguinarine and beberine is not an essential group for antibacterial activity through structure and activity relationships (SARs) analysis. In particular, quaternary ammonium nitrogen in structure was found to be necessary for antibacterial activity. The above findings indicate that it is feasible to simplify the four-membered ring to the planar structure of the three-membered ring.

Based on this, we obtained the mother molecule of 10-methylacridinium by simplifying the skeleton of sanguinarine and berberine. 10-methylacridinium is a conjugate rigid plane structure with polar quaternary ammonium center, which is easily accessible in 2–3 synthetic steps. We attempted to strengthen the rigidity and planarity to fit the binding site of FtsZ better and investigate the effect of side chain on antibacterial activity by introducing various substituents at the C-9 position of the scaffold. In this research, we originally linked the aliphatic amine or substituted aromatic amine to 10-methylacridinium to obtain 10-methyl-9-(alkylamino)acridin-10-ium and 10-methyl-9-(arylalkylamino)acridin-10-ium derivatives (Series A), respectively. We expect to form additional hydrogen bonds of the imine linkers with surrounding amino acid residues in the narrow cleft of FtsZ to increase antibacterial activity. And then, we introduced substituted phenyl, styrene and phenylacetylene at the C-9 position of the scaffold to get 10-methyl-9-arylacridin-10-ium, (*E*)-10-methyl-9-styrylacridin-10-ium and 10-methyl-9-(phenylethynyl)acridin-10-ium derivatives (Series B, C and D), respectively. The linker of Series B is carbon-carbon single bond possessing enough flexibility, which makes the aromatic ring at the C-9 position rotate freely in the narrow cleft to form new binding force. The linker of Series C is carbon-carbon double bond, which urges the aromatic substituents to extend deep into the narrow cleft. We expected that the aromatic substituents could interacted with LEU200, ILE201, VAL203, VAL207, LEU209 in the narrow cleft through hydrophobic interaction. Besides, double bonds can change the density of the electron cloud in the mother molecule, which might affect the antibacterial activity through changing the capability for cationic ionization. Compared with that of Series C, the linker of Series D is carbon-carbon triple bond and the overall structure of this series is linear. This linear skeleton is beneficial for entering the narrow cleft to interact with the amino

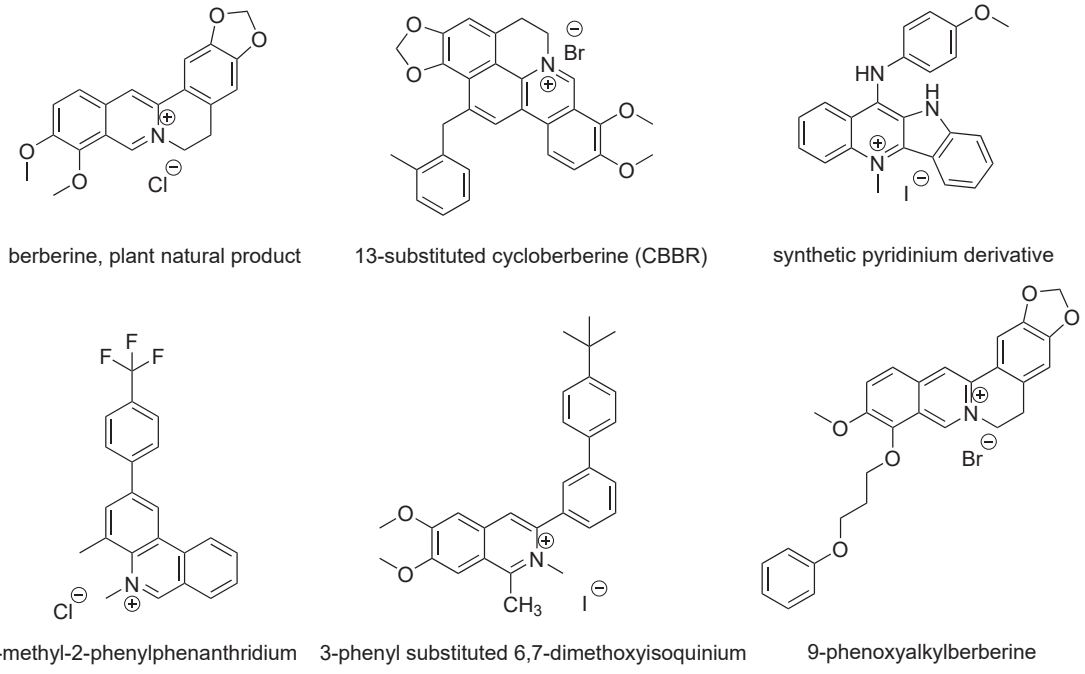

Fig. 1. Chemical structures of some FtsZ inhibitors.

acid residues in the deep. The above brief design strategy is illustrated in Fig. 2.

Here, we systematically designed, synthesized and screened a focused compound library of 61 candidates (Series A, B, C and D) for their antibacterial activity and identified a new class of FtsZ inhibitors. The *in vitro* antibacterial activity against a panel of Gram-positive and Gram-negative bacteria strains including MRSA and VRE was evaluated by testing their MIC values. Bactericidal or bacteriostatic activity was assessed by testing their minimum bactericidal concentration (MBC) and MBC/MIC ratio was calculated to determine their bacteriostatic action. Further, time-kill kinetics was researched to clarify the sterilization of the promising compounds in each time period. Besides, we studied the effect on biofilm formation of *Pseudomonas aeruginosa* to explain the reason of weak activity against Gram-negative bacteria and potential resistance development as an important indicator was evaluated to observe the occurrence of drug resistance. More importantly, the cell morphology of *Bacillus pumilus*, FtsZ polymerization, the assembly and bundling of FtsZ protofilaments as on-target effect were also investigated. The outstanding compound was selected to further evaluate its hemolysis and *in vivo* efficacy. Finally, the interaction mode between those synthesized molecules with FtsZ was revealed through the docking analysis with a reported crystal structure of *Sa*FtsZ (PDB code: 4DXD).

2. Chemistry

The synthetic route for 10-methyl-9-(alkylamino)acridin-10-ium and 10-methyl-9-(arylalkylamino) acridin-10-ium derivatives (Series A) is illustrated in Scheme 1. Commercially available 2-bromobenzoic acid reacted with aniline, affording *N*-phenylanthranilic acid **2** in the presence of excess Cu powder as a catalyst by employing the Ullmann reaction [27]. The acid was cyclizated using concentrated sulfuric acid to afford acridone **3** [28]. *N*-methylacridone **4** was attained by nucleophilic substitution reaction of **3** with iodomethane [29]. Chlorination of **4** using dichlorosulfoxide as solvent furnished key intermediate **5** [30]. 10-methyl-9-(alkylamino)acridin-10-ium and 10-methyl-9-(arylalkylamino) acridin-10-ium derivatives (**6a**-**6w**) were then synthesized via the nucleophilic substitution reaction of freshly prepared chloride **5** with various substituted amines in good yields.

The synthetic route for 10-methyl-9-arylacridin-10-ium derivatives (Series B) is outlined in Scheme 2. 9-Bromoacridine **7** was prepared by the treatment of **3** using phosphorus tribromide as solvent in a good yield [31]. The 9-arylacridin derivatives were easily accessible in one-pot in good yields by employing the Suzuki coupling reaction of **7** with various arylboronic acids in the presence of Pd [0] as catalyst. 10-methyl-9-arylacridin-10-ium derivatives (**9a**-**9o**) were then synthesized via the nucleophilic substitution reaction of various substituted acridines (**8a**-**8o**) with iodomethane in good yields.

(*E*)-10-Methyl-9-styrylacridin-10-ium derivatives (Series C) was synthesized from *N*,*N*-diphenylamine as outlined in Scheme 3. Commercially available **10** was cyclizated with acetic acid to afford the 9-methylacridine **11** [32]. Bromination of **11** in the presence of NBS by employing AIBN as initiator of the free radical reaction furnished the corresponding product **12** in a good yield [33]. The triethyl phosphite first reacted with the **12** by employing the Arbuzov reaction to obtain key intermediate **13**. Then, **13** generated a phosphine ylide under the action of a strong base (NaH), undergoing one-pot reaction with various substituted benzaldehydes via Horner-Emmons reaction to obtain the corresponding products **14a**-**14m**. Methylation of **14a**-**14m** generated the title compounds (*E*)-10-methyl-9-styrylacridin-10-ium derivatives (**15a**-**15m**) using iodomethane, following the similar process as described in Scheme 2.

As shown in Scheme 4, the chemical synthesis of 10-methyl-9-(phenylethynyl)acridin-10-ium derivatives (Series D) was initiated with 9-bromoacridine **7** by employing the Sonogashira coupling reaction in the presence of Pd [II] and Cu [I] as catalysts in a good yield [34]. 10-methyl-9-(phenylethynyl)acridin-10-ium derivatives (**17a**-**17j**) were obtained through methylation of **16a**-**16j**, according to similar procedure as described in Scheme 2.

3. Results and discussions

3.1. In vitro antibacterial activity of 9-arylalkyl-10-methylacridinium derivatives

The synthesized compounds were initially tested against eight

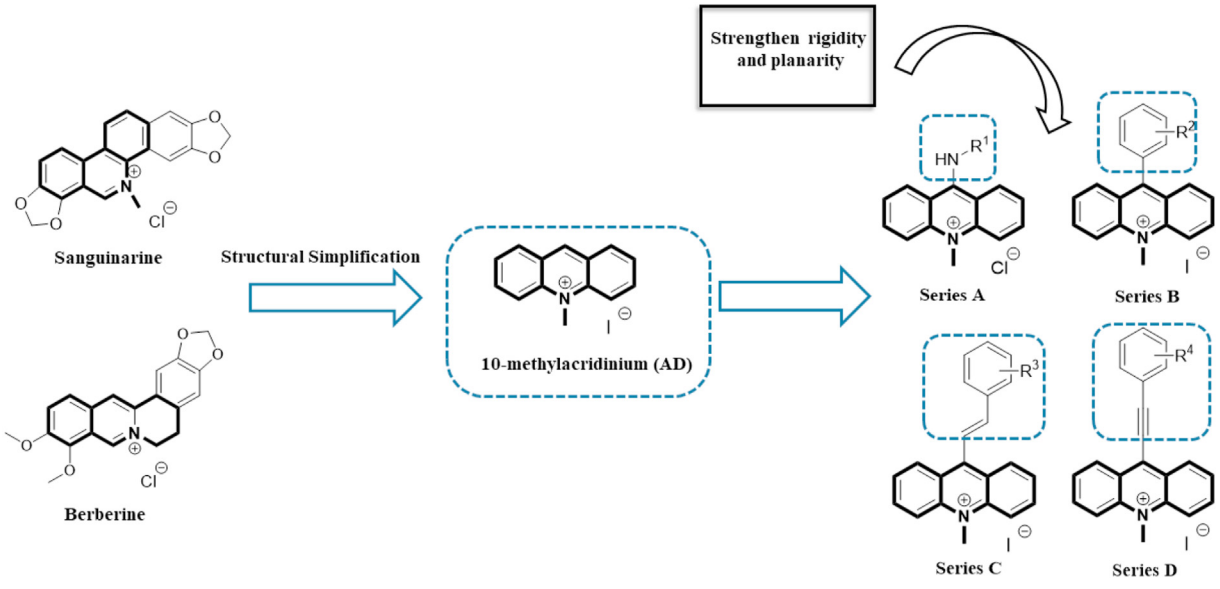

Fig. 2. Brief design process of the 9-arylalkyl-10-methylacridinium derivatives.

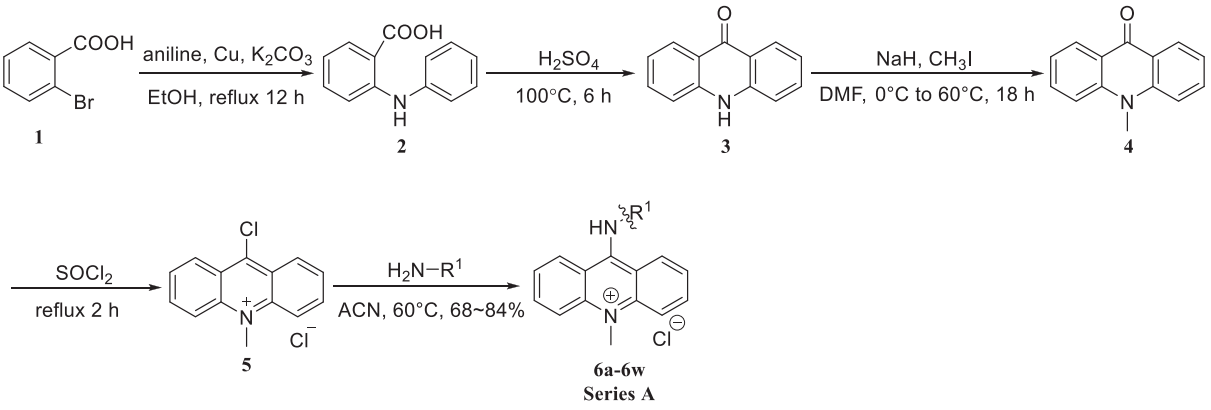

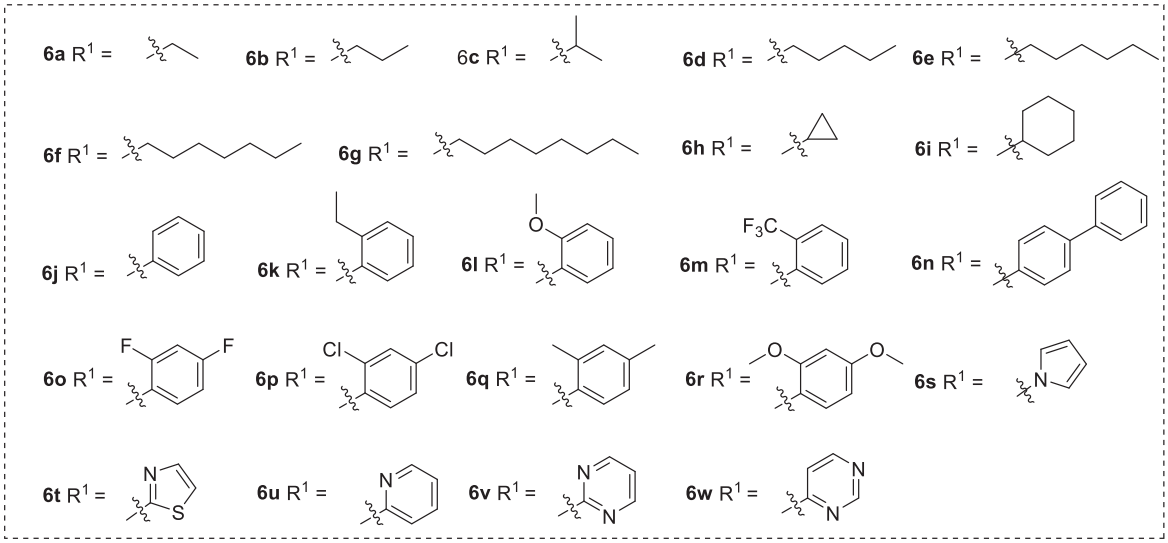

Scheme 1. Synthesis of 10-methyl-9-(alkylamino)acridin-10-ium and 10-methyl-9-(arylalkylamino) acridin-10-ium derivatives.

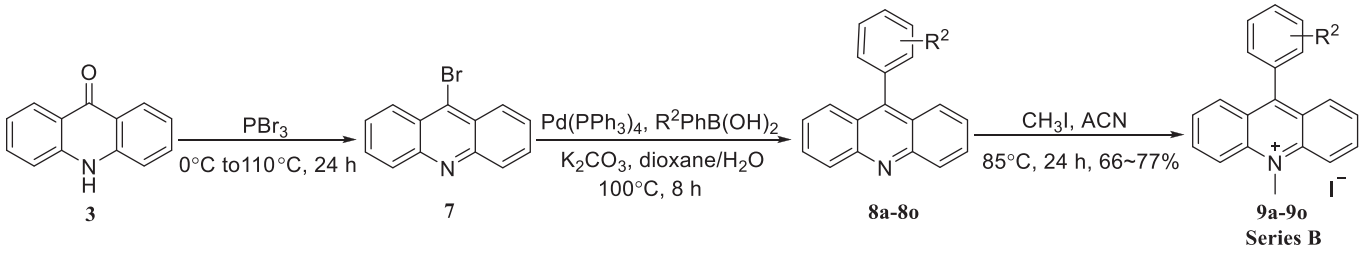

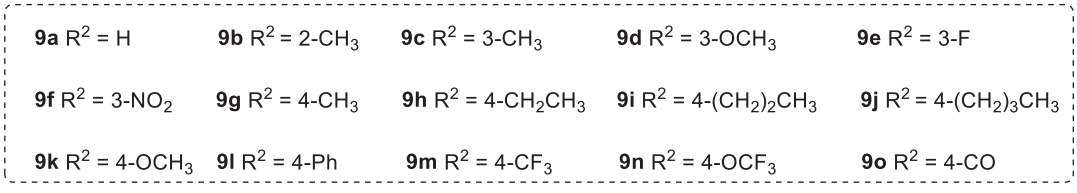

Scheme 2. Synthesis of 10-methyl-9-arylacridin-10-ium derivatives.

susceptible bacteria strains, including *B. subtilis* ATCC9372, *B. pumilus* CMCC63202, *S. aureus* ATCC25923, *Streptococcus pyogenes* 1, *Enterococcus faecalis* ATCC29212, *Enterococcus faecium* ATCC19434, *P. aeruginosa* ATCC27853 and *Escherichia coli* ATCC25922, and seven resistant bacteria strains, including *S. aureus* ATCC43300, *S. aureus* PR, *S. aureus* CI, *Staphylococcus epidermidis*, *S. pyogenes* 2, *E. faecalis* ATCC51299 and *E. faecium* ATCC51559. Sanguinarine (San), berberine (Ber), ciprofloxacin (Cip), linezolid (Lin) and vancomycin (Van) were used as controls to compare the effect of various linkers and substituents of the synthesized

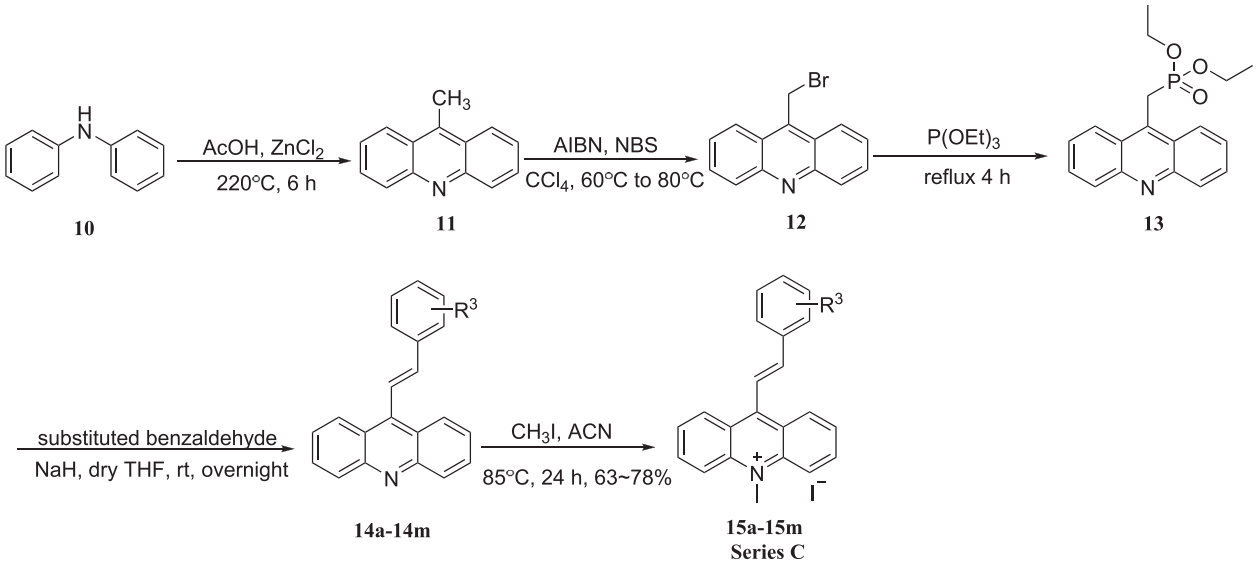

15a R^3 = H **15b** R^3 = 2-OCH_3 **15c** R^3 = 4-CH_3 **15d** R^3 = 4-CH_2CH_3 **15e** R^3 = 4-$(CH_2)_3CH_3$

15f R^3 = 4-$CH(CH_3)_3$ **15g** R^3 = 4-OCH_2CH_3 **15h** R^3 = 3,4-di-OCH_3 **15i** R^3 = 4-Ph

15j R^3 = 4-F **15k** R^3 = 4-Cl **15l** R^3 = 4-Br **15m** R^3 = 2,4-di-Cl

Scheme 3. Synthesis of (*E*)-10-methyl-9-styrylacridin-10-ium derivatives.

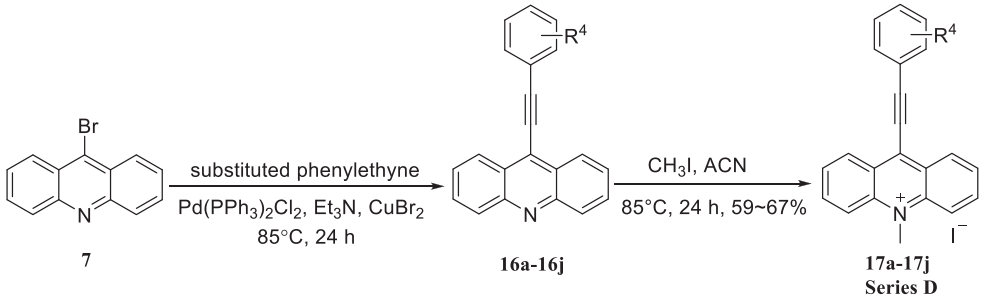

17a R^4 = H **17b** R^4 = 2-CH_3 **17c** R^4 = 2-OCH_3 **17d** R^4 = 3-CH_3 **17e** R^4 = 4-CH_2CH_3

17f R^4 = 4-$(CH_2)_3CH_3$ **17g** R^4 = 4-OCH_3 **17h** R^4 = 4-OCH_2CH_3 **17i** R^4 =4-$O(CH_2)_2CH_3$ **17j** R^4 = 4-Ph

Scheme 4. Synthesis of 10-methyl-9-(phenylethynyl)acridin-10-ium derivatives.

compounds on antibacterial activity. Their MIC values were listed in Tables 1 and 2.

3.1.1. In vitro antibacterial activity of Series A analogues

The target compounds of Series A were evaluated for *in vitro* antibacterial activity (Tables 1 and 2). The results demonstrated that only **6f**, **6g**, **6s** and **6w** showed inhibitory effect on the tested bacterial strains. Among them, **6g** with 8-carbon alkyl chain exhibited the moderate activity against the four tested susceptible bacterial strains of *B. subtilis* ATCC9372, *B. pumilus* CMCC63202, *S. aureus* ATCC25923 and *S. pyogenes* 1 with the MIC values of 16, 16, 8 and 16 μg/mL, respectively. On the other hand, **6g** also inhibited the growth of resistant bacterial strains of *S. aureus* PR and *S. aureus* CI with the MIC values of 4 and 8 μg/mL, respectively. **6f** possessing 7-carbon alkyl chain not only performed moderate activity against *S. aureus* ATCC25923 and *S. pyogenes* 1 with an MIC value of 16 μg/mL, but also offered the activity against resistant bacterial strains of *S. aureus* PR and *S. aureus* CI. Besides, **6s** with pyrrole ring and **6w** with pyrimidine ring showed weak activity against some Gram-positive bacterial strains.

Based on the above MIC data, the structure-activity relationships (SARs) of Series A were summarized as follows. Introduction of a long unbranched alkyl chain contributed to the increased antibacterial activity (see **6a**-**6g**). The antibacterial activity of **6g** (8-carbon alkyl chain) was stronger than that of **6f** (7-carbon alkyl chain), which was induced by the lengthening of the side chain. We

Table 1
In vitro antibacterial activity against susceptible-bacteria of Series **A**, **B**, **C** and **D** (**6a-6w**, **9a-9o**, **15a-15m** and **17a-17j**).

Comp	Minimum Inhibitory Concentration/MIC (μg/mL)							
	B. subtilis ATCC9372[a]	*B. pumilus* CMCC63202[b]	*S. aureus* ATCC25923[c]	S.pyogenes 1[d]	*E. faecalis* ATCC29212[e]	*E. faecium* ATCC19434[f]	*P. aeruginosa* ATCC27853[g]	*E. coli* ATCC25922[h]
6a	64	>64	>64	64	NT	NT	>64	>64
6b	>64	>64	>64	32	NT	NT	>64	>64
6c	>64	>64	>64	>64	NT	NT	>64	>64
6d	64	>64	>64	16	NT	NT	>64	>64
6e	64	64	64	32	NT	NT	>64	>64
6f	32	32	16	16	NT	NT	>64	>64
6g	16	16	8	16	NT	NT	>64	>64
6h	>64	>64	>64	>64	NT	NT	>64	>64
6i	32	>64	>64	>64	NT	NT	>64	>64
6j-6r	>64	>64	>64	>64	NT	NT	>64	>64
6s	64	64	32	16	NT	NT	>64	>64
6t	>64	>64	>64	>64	NT	NT	>64	>64
6u	64	>64	>64	>64	NT	NT	>64	>64
6v	>64	>64	>64	>64	NT	NT	>64	>64
6w	16	64	16	>64	NT	NT	>64	>64
9a	16	32	2	8	NT	NT	>64	>64
9b	32	>64	8	64	NT	NT	>64	>64
9c	8	16	1	4	NT	NT	>64	>64
9d	16	32	4	8	NT	NT	>64	>64
9e	16	32	8	4	NT	NT	>64	>64
9f	64	>64	16	16	NT	NT	>64	>64
9g	4	8	1	4	NT	NT	>64	>64
9h	2	4	0.25	2	NT	NT	>64	>64
9i	1	2	0.25	1	NT	NT	>64	>64
9j	0.5	1	0.03	1	4	4	>64	64
9k	8	16	4	8	NT	NT	>64	>64
9l	1	1	0.125	0.5	4	4	>64	64
9m	4	16	1	1	NT	NT	>64	>64
9n	4	8	0.5	1	NT	NT	>64	>64
9o	>64	>64	64	64	NT	NT	>64	>64
15a	1	2	0.5	0.25	NT	NT	>64	>64
15b	1	2	0.25	0.25	NT	NT	>64	>64
15c	1	0.5	0.5	0.25	NT	NT	>64	64
15d	1	1	0.5	0.5	NT	NT	>64	64
15e	1	1	1	0.5	NT	NT	>64	>64
15f	0.25	0.5	0.5	<0.125	2	4	>64	>64
15g	2	1	0.5	<0.125	NT	NT	>64	>64
15h	8	16	4	2	NT	NT	>64	>64
15i	1	1	0.5	0.5	NT	NT	>64	32
15j	2	2	1	0.5	NT	NT	>64	>64
15k	2	1	1	1	NT	NT	>64	>64
15l	1	1	0.5	0.25	NT	NT	>64	64
15m	0.5	2	0.5	0.25	2	4	>64	32
17a	2	2	2	4	NT	NT	>64	>64
17b	8	8	4	8	NT	NT	>64	>64
17c	8	8	8	16	NT	NT	>64	>64
17d	2	2	2	4	4	8	>64	>64
17e	2	2	2	4	2	4	>64	>64
17f	4	2	4	8	NT	NT	>64	>64
17g	4	4	4	16	NT	NT	>64	>64
17h	4	4	4	16	NT	NT	>64	>64
17i	4	4	4	16	NT	NT	>64	>64
17j	8	8	8	16	NT	NT	>64	>64
AD	>64	>64	>64	>64	>64	>64	>64	>64
San[i]	4	4	4	2	16	64	64	32
Ber[j]	>64	>64	64	>64	>64	>64	>64	>64
Cip[k]	2	16	4	8	32	>64	8	0.25
Lin[l]	0.5	2	2	1	4	8	>64	>64
Van[m]	0.5	2	1	0.25	4	2	>64	>64

[a] *B. subtilis* ATCC9372*: Bacillus subtilis* ATCC9372, penicillin-susceptible strain.
[b] *B. pumilus* CMCC63202*: Bacillus pumilus* CMCC63202, penicillin-susceptible strain.
[c] *S. aureus* ATCC25923: *Staphylococcus aureus* ATCC25923, erythromycin-susceptible strain.
[d] *S. pyogenes* 1: *Streptococcus pyogenes* 1, erythromycin-susceptible strain isolated clinically.
[e] *E. faecalis* ATCC29212: *Enterococcus faecalis* ATCC29212, vancomycin-susceptible strain.
[f] *E. faecium* ATCC19434: *Enterococcus faecium* ATCC19434, vancomycin-susceptible strain.
[g] *P. aeruginosa* ATCC27853: *Pseudomonas aeruginosa* ATCC27853, penicillin-susceptible strain, not characterized.
[h] *E. coli* ATCC25922: *Escherichia coli* ATCC25922, penicillin-susceptible strain.
[i] San: Sanguinarine.
[j] Ber: Berberine.
[k] Cip: Ciprofloxacin.
[l] Lin: Linezolid.
[m] Van: Vancomycin.

inferred that their lipid/water partition coefficients (logP) as one of the most important factors could affected the activity [35]. Therefore, we theoretically calculated the logP values (ClogP) by the commercial ChemBioOffice 2014 (Cambridge Soft, USA) to further confirm their influence on antibacterial activity. Consequently, the ClogP value of **6g** with 8-carbon alkyl chain was the highest, which suggested the ability of penetrating the lipid bilayer contributed significantly to antibacterial activity. The above results confirmed that the presence of an alkyl group could produce moderate activity. Other compounds with stronger electronegativity state could lead to the loss of antibacterial activity as a result of their poor cell penetration. Besides, we inferred that aniline as substituent in structure could rotate freely in space, which reduced the planarity and made it difficult to enter into a narrow hydrophobic cavity of FtsZ. These findings help us to conduct further structural optimization.

3.1.2. In vitro antibacterial activity of Series B analogues

The MIC data of Series B analogues were exhibited in Tables 1 and 2. The results showed that **9j** possessed equivalent antibacterial activity (0.5 μg/mL) against *B. subtilis* ATCC9372 to that of linezolid and vancomycin, and **9j** and **9l** demonstrated stronger activity against *B. pumilus* CMCC63202 than the controls. Moreover, **9h**, **9i**, **9j**, **9l** and **9n** exhibited 8−133 fold increase in activity against *S. aureus* ATCC25923 compared with the lead compound. The activity of **9i**, **9j**, **9l**, **9m** and **9n** against *S. pyogenes* 1 were comparable to that of linezolid (1 μg/mL) but not better than that of vancomycin (0.25 μg/mL). As for susceptible *enterococcus* strains, **9j** and **9l** showed equivalent antibacterial activity (4 μg/mL) to that of vancomycin. Furthermore, **9j** and **9l** as the promising compounds in this series could inhibit the growth of all the tested resistant bacteria strains including MRSA and VRE with the MIC values ranging from <0.125 to 8 μg/mL, which were comparable or superior to that of the controls.

The SARs of Series B were summarized as follows. The MIC results showed that the antibacterial activity of compound without substituents on the phenyl group (**9a**) was stronger than that of the compounds with C-2 position substituents. Compounds with electron-donating substituents of C-3 position on the phenyl ring (**9c** and **9d**) were only marginally more active than **9a**, whereas electron-withdrawing substituent of C-3 position (**9f**) led to a loss of activity. Surprisingly, compounds with substituents at the C-4 position of the phenyl ring displayed significantly improved activity. For example, **9j** with 4-carbon alkyl chain offered the most potent antibacterial activity. Furthermore, with the extension of alkyl chain, the activity also increased. The above analysis indicated that when there was the same substituent on the phenyl group, its extension direction in space had great effect on the antibacterial activity. Besides, the antibacterial activity of **9l** with biphenyl group was second only to **9j**, which emphasized the importance in planarity of scaffold. In view of this, we inferred that the bulky substituent (**9l** and **9j**) could extend into the binding cavity of FtsZ to form new binding force. Thus, it was necessary to lengthen the linker to two carbons, and keep the mother nucleus and substituents on the same plane.

3.1.3. In vitro antibacterial activity of Series C analogues

The antibacterial activity of Series C was showed in Tables 1 and 2. All the test compounds except for **15h** exhibited excellent antibacterial activity against Gram-positive bacteria, some of which were better than control drugs in antibacterial activity. Among them, **15f** as the most promising compound showed excellent activity against the six tested susceptible bacterial strains of *B. subtilis* ATCC9372, *B. pumilus* CMCC63202, *S. aureus* ATCC25923, *S. pyogenes* 1, *E. faecalis* ATCC29212 and *E. faecium* ATCC19434 with the MIC values of 0.25, 0.5, 0.5, <0.125, 2 and 4 μg/mL, respectively. Besides, **15f** displayed strong activity against MRSA, *S. epidermidis*, *S. pyogenes* 2 and VRE, better than or equal to control drugs. Similarly, **15m** not only exerted the excellent activity against *B. subtilis* ATCC9372 and *S. aureus* ATCC25923 with a low MIC value of 0.5 μg/mL but also effectively inhibited the growth of three resistant *S. aureus* strains and VRE.

The SARs of Series C were summarized below. The antibacterial activity of compounds with C-2 and C-4 position substituents were similar to that of **15a** (no substituent on the phenyl ring), which indicated that the extension direction of the substituents in space had little effect on antibacterial activity. In particular, **15f** containing a *tert*-butyl side chain demonstrated the best antibacterial activity, which suggested that the appropriate length and flexibility more easily generated hydrophobic interaction with the binding site of FtsZ. In addition, **15f** had a higher ClogP value (3.087) than the other compounds, which was also beneficial for the compound to penetrate the bacterial cell membrane. In contrast, decreasing the chain lipophilicity by introducing an oxygen atom (**15g** and **15h**) on the phenyl ring or introducing the electron-donating substituents (**15j** and **15k**) led to decreased antibacterial activity.

3.1.4. In vitro antibacterial activity of Series D analogues

The antibacterial activity of Series D was showed in Tables 1 and 2 In Series D, **17a**, **17d** and **17e** showed inhibitory effect on the four tested susceptible bacterial strains of *B. subtilis* ATCC9372, *B. pumilus* CMCC63202, *S. aureus* ATCC25923 and *S. pyogenes* 1 with the MIC values of 2, 2, 2 and 4 μg/mL, respectively. It was worth mentioning that **17e** exhibited remarkable activity against *E. faecalis* ATCC29212 with a MIC value of 2 μg/mL, which was 2-fold more potent than that of vancomycin. Especially, **17d** exhibited the best activity against all the tested resistant bacteria, with the MIC values ranging from 2 to 8 μg/mL, better than or equal to sanguinarine, ciprofloxacin, linezolid and vancomycin.

The SARs of Series D indicated that the C-3 and C-4 position substitutions on the phenyl ring demonstrated improved antibacterial activity over a C-2 substituted scaffold. Besides, introducing an oxygen atom (**17g**, **17h** and **17i**) on the phenyl ring led to decreased antibacterial activity compared with introducing an alkyl chain (**17e** and **17f**).

In general, Series C (substituted with alkene) as the most outstanding series demonstrated excellent antibacterial activity against all the susceptible and resistant Gram-positive bacterial strains, some of which were better than control drugs. Among them, **15f** showed a strong inhibitory effect on the susceptible and resistant bacterial strains including MRSA and VRE with the MIC values ranging from <0.125 to 4 μg/mL. All the compounds in Series D (substituted with alkyne) performed good antibacterial activity against all the tested Gram-positive bacterial strains, but on the whole they were not as good as those in Series C. In addition, **15a** (no substituent on the phenyl ring) in Series C and **17a** (no substituent on the phenyl ring) in Series D had satisfactory activity with the MIC values ranging from 0.25 to 8 μg/mL, which indicated the introduction of substituents had little effect on the antibacterial activity. The compounds in Series B (substituted with phenyl) made a big difference in antibacterial activity and the introduction of substituent on the phenyl ring affected the activity significantly. Among them, **9j** with 4-carbon alkyl chain could exert excellent antibacterial activity with the MIC values ranging from 0.03 to 8 μg/mL. The antibacterial activity of Series B to susceptible bacteria is good, but barely satisfactory to resistant bacteria. In Series A, **6f**, **6g**, **6s** and **6w** showed inhibitory effect on the tested bacterial strains. Among them, **6f** with 7-carbon alkyl chain and **6g** with 8-carbon alkyl chain displayed moderate antibacterial activity against the four tested susceptible bacterial strains, which confirmed that the

Table 2
In vitro antibacterial activity against resistant-bacteria of Series **A**, **B**, **C** and **D** (**6a-6w**, **9a-9o**, **15a-15m** and **17a-17j**).

Comp	Minimum Inhibitory Concentration/MIC (μg/mL)						
	S. aureus ATCC43300[a]	*S. aureus* PR[b]	*S. aureus* CI[c]	S. epidermidis[d]	S. pyogenes2[e]	*E. faecalis* ATCC51299[f]	*E. faecium* ATCC51559[g]
6a	>64	>64	>64	>64	64	NT	NT
6b	>64	>64	>64	64	64	NT	NT
6c	>64	>64	>64	>64	>64	NT	NT
6d	>64	64	>64	64	32	NT	NT
6e	64	64	64	64	32	NT	NT
6f	32	16	16	32	32	NT	NT
6g	16	4	8	16	16	NT	NT
6h	>64	>64	>64	>64	64	NT	NT
6i	>64	>64	>64	>64	64	NT	NT
6j-6r	>64	>64	>64	>64	>64	NT	NT
6s	>64	64	64	64	64	NT	NT
6t	>64	>64	>64	>64	>64	NT	NT
6u	>64	>64	>64	>64	>64	NT	NT
6v	>64	>64	>64	>64	>64	NT	NT
6w	32	>64	32	>64	>64	NT	NT
9a	>64	>64	8	>64	32	NT	NT
9b	>64	>64	64	>64	>64	NT	NT
9c	64	>64	4	64	16	NT	NT
9d	>64	>64	8	>64	32	NT	NT
9e	>64	>64	16	>64	16	NT	NT
9f	64	>64	32	>64	64	NT	NT
9g	64	>64	4	64	16	NT	NT
9h	16	64	1	32	4	NT	NT
9i	4	16	0.25	8	4	NT	NT
9j	2	8	<0.125	2	2	4	2
9k	>64	>64	8	>64	16	NT	NT
9l	2	8	0.25	2	1	4	2
9m	16	64	2	32	2	NT	NT
9n	32	64	2	32	4	NT	NT
9o	>64	>64	>64	>64	>64	NT	NT
15a	4	8	2	8	0.5	NT	NT
15b	4	16	1	8	0.5	NT	NT
15c	4	8	1	2	0.5	NT	NT
15d	2	8	1	4	1	NT	NT
15e	8	8	2	2	0.5	NT	NT
15f	1	2	0.5	1	0.25	4	2
15g	2	8	1	4	0.5	NT	NT
15h	16	64	8	32	4	NT	NT
15i	2	4	1	2	0.5	NT	NT
15j	8	16	2	8	0.5	NT	NT
15k	2	4	2	2	1	NT	NT
15l	2	4	1	2	0.5	NT	NT
15m	1	2	1	2	0.5	8	4
17a	2	4	2	4	8	NT	NT
17b	4	8	2	16	16	NT	NT
17c	8	16	4	16	16	NT	NT
17d	2	2	2	4	4	8	4
17e	2	4	2	8	4	8	4
17f	4	8	4	8	8	NT	NT
17g	8	16	4	16	16	NT	NT
17h	4	8	4	8	8	NT	NT
17i	4	16	4	8	16	NT	NT
17j	16	16	16	8	16	NT	NT
AD	>64	>64	>64	>64	>64	>64	>64
San	8	16	8	8	2	32	32
Ber	>64	>64	>64	>64	64	>64	>64
Cip	16	>64	16	>64	>64	>64	>64
Lin	2	4	2	4	1	4	4
Van	4	2	NT	4	1	>64	>64

[a] *S. aureus* ATCC43300: *Staphylococcus aureus* ATCC43300, methicillin-resistant strain.
[b] *S. aureus* PR: *Staphylococcus aureus* PR, penicillin-resistant strain.
[c] *S. aureus* CI: *Staphylococcus aureus*, clinical isolated strain, not characterized.
[d] *S. epidermidis: Staphylococcus epidermidis*, penicillin-resistant strain isolated clinically, not characterized.
[e] *S. pyogenes* 2: *Streptococcus pyogenes* 2, erythromycin-resistant strain isolated clinically.
[f] *E. faecalis* ATCC51299: *Enterococcus faecalis* ATCC51299, vancomycin-resistant strain.
[g] *E. faecium* ATCC51559: *Enterococcus faecium* ATCC51559, vancomycin-resistant strain.

presence of an alkyl group gave moderate activity. The order of antibacterial activity of the four series is Series C > Series D > Series B > Series A. Series A containing substituted amines could rotate flexibly in space, whereas the narrow cleft binding site required some degree of planarity in order to fit better. Increasing the scaffold rigidity by the introduction of alkene (Series C) and alkyne

(Series D) strengthened antibacterial activity, which contributed to penetrating into the hydrophobic cavity of FtsZ forming hydrogen bond interaction, π-π stacking interaction, electrostatic interaction and hydrophobic interaction. Besides, prolonging the linker to two carbons contributed to the increased activity. This might be because compounds suit the hydrophobic cavity of FtsZ better, thereby strengthening affinity for FtsZ. In summary, lengthening the linker, and keeping the mother nucleus and substituents on the same plane were crucial to antibacterial activity. It was worth mentioning that all the series except for Series A demonstrated increased antibacterial activity, as compared to the mother molecule (AD), which was corresponding to our optimization strategy. In the next assays, **15f** as the most potent compound was selected for further evaluation.

3.2. Bactericidal or bacteriostatic activity

To further investigate whether its antibacterial activity was bactericidal or bacteriostatic, we determined the MBC of **15f** against three susceptible bacteria strains (*S. aureus* ATCC25923, *B. subtilis* ATCC9372 and *B. pumilus* CMCC63202) and three resistant bacteria strains (*S. aureus* ATCC43300, *S. aureus* PR and penicillin-resistant *S. epidermidis*). Sanguinarine and linezolid were used as controls in the MBC determinations. According to the Clinical and Laboratory Standards Institute (CLSI) standards, an MBC/MIC ratio $\leq$ 4 is regarded as a bactericidal behavior. The results shown in Table 3 indicate that the MBC/MIC ratios of sanguinarine and linezolid are $\geq$8, which were observed as bacteriostatic activity. By contrast, **15f** was observed as a bactericidal agent with the MBC/MIC ratios $\leq$4. Significantly, **15f** exhibited almost identical MBC and MIC values (i.e. MBC/MIC ratio = 1 or 2) for both susceptible and resistant bacterial strains, indicating its bactericidal mode clearly.

3.3. Kinetics of the bactericidal activity

The time-kill kinetic approach against *S. aureus* ATCC25923 was used to investigate the kinetics of the bactericidal activity. As shown in Fig. 3, the bacteria increased sharply in the counts of CFU without **15f** or in the presences of 0.5 × MIC of **15f**. By contrast, **15f** achieved a 2.2 log reduction in initial bacterial load (more than 99.99% of bacteria were killed) in 3 h at 4 × MIC, and a 2.43 log CFU reduction in 24 h at 2 × MIC. It was noteworthy that the commercial antibiotic linezolid at 16 × MIC achieved approximately same killing efficacy to **15f** at 1 × MIC. Fast bactericidal performance would shorten the treatment time, which could reduce the probability of bacterial resistance. These findings revealed that **15f** could serve as an excellent bactericidal agent in a concentration-dependent manner.

3.4. Effect on biofilm formation of P. aeruginosa

The antibacterial activity of the test compounds against Gram-negative bacteria was much weaker than that against Gram-positive bacteria. One potential explanation is that the lipopolysaccharide (LPS) layer outside the cell membrane of Gram-negative bacteria could prevent the entry of the compounds and result in the very low permeability of membrane. Moreover, biofilm plays an essential role in drug resistance as well. Thus, **15f** was selected to measure its effect on *P. aeruginosa* ATCC27853 biofilm formation using the crystal violet assay [36]. As shown in Fig. 4, the inhibition rate of the *P. aeruginosa* ATCC27853 biofilm formation was very similar to the negative control even though the concentration of **15f** reached to 64 μg/mL. This result showed that **15f** was impossible to inhibit the biofilm formation of *P. aeruginosa* ATCC27853, thereby demonstrating that it had no antibacterial activity against Gram-negative bacteria.

3.5. Evaluation of potential resistance development

Bacterial resistance to the currently used antimicrobials is a major cause of ineffective treatment of infectious diseases [37,38]. Thus, the evaluation of potential resistance development is necessary in developing new antimicrobials [39,40]. The propensity of bacterial resistance development for **15f** was performed using a multipassage resistance selection assay. We passaged *S. aureus* ATCC25923 at subinhibitory concentration (0.5 × MIC) of **15f** and ciprofloxacin for 18 cycles. As shown in Fig. 5, no greater than a 2-fold increase in the MIC values was observed for **15f** after 18 passages, while the MIC value of ciprofloxacin was increased by 64-fold after 9 passages. These results demonstrated that **15f** could avoid inducing bacterial resistance. We inferred that new antibacterial mechanism and the rapid bactericidal pattern of **15f** played an important role in overcoming the emergence of bacterial resistance.

3.6. Effects on the morphology of B. pumilus cells

Berberine and benzamide FtsZ inhibitors is known to disrupt FtsZ activity and then cause the morphology of bacteria to grow larger or longer [22,41,42]. Because the combination of those compounds with FtsZ inhibits the normal function of FtsZ, and then hinders bacterial division process. Increasing or prolonged bacterial cell volume eventually leads to bacterial lysis and death. Thus, we used an optical microscope to observe the bacterial morphology of *B. pumilus* cultured with or without **15f**. Cell morphological changes are shown in Fig. 6. The result showed that **15f** significantly increased the length of *B. pumilus* compared to the control. For example, the normal cell length of *B. pumilus* cells is around 1.2−3 μm (Fig. 6A), while the cell length after incubated with 0.5 × MIC concentration (0.25 μg/mL) was longer than 20 μm (Fig. 6B). These cell elongation phenomena were similar to that of other known FtsZ inhibitors, indicating preliminarily its inhibitory effect on FtsZ.

3.7. Stimulation of FtsZ polymerization dynamics

Research on the dynamic of FtsZ has demonstrated that some FtsZ-targeting inhibitors can stimulate the polymerization of FtsZ and stabilize the structure of FtsZ polymer, which is beneficial for improving the antibacterial activity of FtsZ inhibitors [43,44]. The antibacterial activity of sanguinarine and berberine might owe to their inhibitory effect on the polymerization of FtsZ [16,17,45]. Thus, we selected **15f** for testing on the polymerization of purified *B. subtilis* FtsZ (*Bs*FtsZ) *in vitro*. For this assay, we utilized a light scattering approach to detect the effect of **15f** on the FtsZ polymerization. Fig. 7 showed the time-dependent polymerization profiles of *Bs*FtsZ in the absence and in the presence of **15f** at different concentrations ranged from 2.5 to 10 μg/mL. Moreover, the time-dependent light scattering intensity illustrated in Fig. 7 revealed that **15f** stimulated the kinetics of *Bs*FtsZ polymerization in a concentration-dependent manner. As expected, both linezolid (10 μg/mL) and DMSO vehicle had a negligible effect on the polymerization of *Bs*FtsZ. This different stimulatory impact on FtsZ polymerization indicated that **15f** exerted antibacterial activity through interacting with the FtsZ.

3.8. Promoting the assembly and bundling of FtsZ protofilaments

Apart from the light scattering assay, the effect of **15f** on the polymerization of FtsZ were further analyzed by transmission

electron microscopy (TEM) to investigate the morphological change of FtsZ filaments. As shown in Fig. 8, short, thin and single strand FtsZ filaments were observed in the absence of the test compound. After treated with 10 μg/mL of **15f**, the size and thickness of the FtsZ polymers substantially increased, implying that this compound stimulated the formation of bundling of the FtsZ protofilaments in a longitudinal and lateral manner. As expected, high efficacy of promoting both the assembly of *Bs*FtsZ and bunding of *Bs*FtsZ polymers were observed for **15f**, which was in accordance with its result of light scattering assay.

3.9. Evaluation of potential hemolysis

15f containing quaternary ammonium nitrogen might disrupt mammalian cell membrane. In order to determine whether it was cytotoxic to mammalian cells, the hemolysis assay was performed with mouse red blood cells. 2% Triton X-100 was selected as a positive control and the results were displayed in Fig. 9. When tested at the concentration of 2 × MIC, **15f** barely exhibited hemolysis (0.71%). With the increase of the tested concentration, however, its potential hemolysis also heightened. Nevertheless, **15f** only displayed 9.89% hemolysis even though its concentration reached to 16 × MIC. All hemolysis levels were below 10%, which indicated that **15f** was not significantly hemolytic within the range of its antibacterial concentration. These findings encouraged us to explore its *in vivo* efficacy.

3.10. In vivo efficacy against murine bacterial infection model

In view of its excellent *in vitro* antibacterial activity, **15f** was further assessed for *in vivo* efficacy using murine bacteremia model, which are commonly used to evaluate the systemic effects of antibiotics [46]. Thus, murine bacteremia model was established by intraperitoneal injection with about 10^7 CFU/mL of the *S. aureus* ATCC25923 solution, and 0.9% saline was injected as a negative control group. The treatment was performed after the 1-h injection, which is sufficient for the bacteria to spread throughout the mouse [47] and then, mice were intraperitoneally treated with different doses of **15f** and linezolid dissolved in vehicle. As shown in Fig. 10,

Table 3
Comparison of MIC and MBC values for **15f** in six Gram-positive bacteria strains.

Comp	MBC (μg/mL)	MIC (μg/mL)	MBC/MIC
	Susceptible *S. aureus* (ATCC25923)		
15f	2	0.5	4
San	>64	2	>32
Lin	4	0.125	32
	Methicillin-resistant *S. aureus* (ATCC43300)		
15f	4	1	4
San	>64	2	>32
Lin	NT	>64	NT
	Penicillin-resistant *S. aureus* PR		
15f	4	2	2
San	128	16	8
Lin	16	4	4
	Susceptible *B. subtilis* (ATCC9372)		
15f	0.5	0.25	2
San	64	4	16
Lin	64	0.5	128
	Susceptible *B. pumilus* (CMCC63202)		
15f	2	0.5	4
San	>64	1	>64
Lin	NT	>64	NT
	Penicillin-resistant *S. epidermidis*		
15f	1	1	1
San	64	1	64
Lin	NT	>64	NT

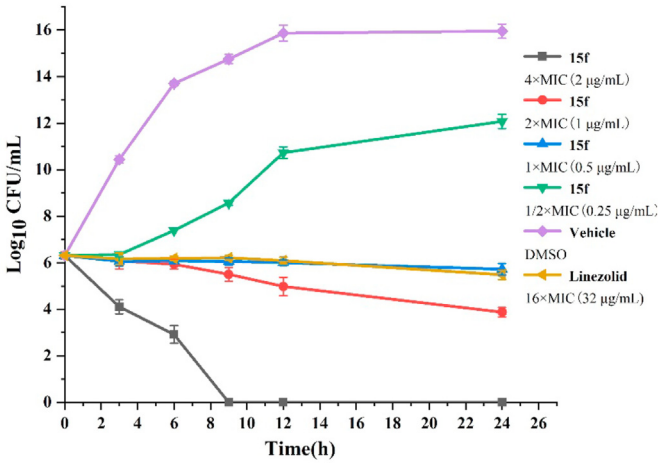

Fig. 3. Time-kill curves of compound **15f** against *S. aureus* ATCC25923. Each data point reflects the average of two independent measurements, with the error bars reflecting the standard deviation from the mean.

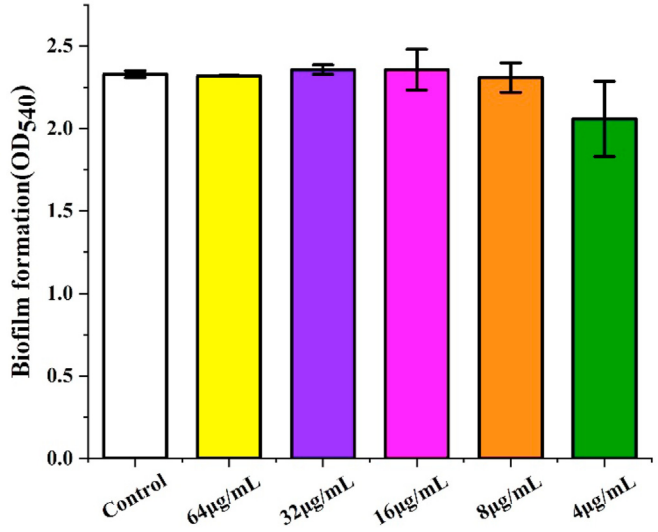

Fig. 4. 18 h biofilm biomass was measured by the crystal violet assay of *P. aeruginosa* ATCC27853 bacterial culture and different concentrations of the test compound **15f** (Values are presented as the mean ± SD, n = 3).

15f at 25 mg/kg significantly reduced the bacterial load compared with the no drug control group, and the difference was statistically significant ($P < 0.001$). Contrarily, **15f** at 1 mg/kg could not inhibit the growth of bacteria. We inferred that this was related to its metabolism *in vivo*. Furthermore, **15f** could reduce the number of viable pathogens of infected mice at medium dosage (5 mg/kg), and its efficacy was as good as that of linezolid at the same concentration. Although **15f** showed better efficacy at high dosage, linezolid demonstrated better *in vivo* antibacterial activity than **15f**. These results suggested that **15f** possessed therapeutic potential as a novel antibacterial agent.

3.11. Computational studies of the binding mode

To gain more insights into the interaction mode of **15f** with FtsZ, computational docking studies were conducted using the reported crystal structure of *S. aureus* FtsZ (PDB ID: 4DXD). The docking results demonstrated that **15f** was inclined to bind near the T7-loop

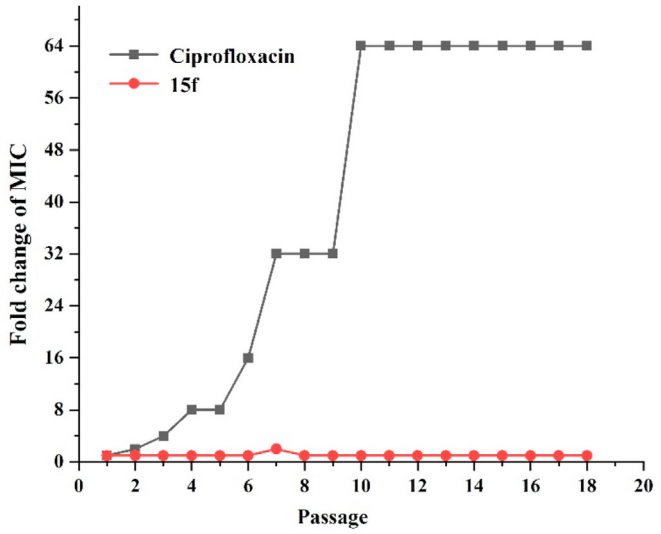

Fig. 5. Bacterial resistance studies of compound **15f** and ciprofloxacin against *S. aureus* ATCC25923.

(Fig. 11A). This binding site is a narrow hydrophobic cavity surrounded by H7-helix, T7-loop, and a four-stranded β-sheet. This narrow hydrophobic cavity required a certain degree of planarity, which was in good agreement with configuration of **15f** through hydrophobic interactions. The side chain of **15f** extended into the depth of cavity forming hydrophobic interaction with LEU200, VAL203, VAL207 and ILE201. Furthermore, quaternary ammonium center of **15f** was hydrophilic, which interacted with the surrounding amino acid residues through an electrostatic interaction or van der waals force with GLN192, GLY193 and GLY227. (Fig. 11B). The docking result revealed **15f** suited the hydrophobic cavity of FtsZ perfectly, which was consistent with our design strategy.

4. Conclusion

In summary, four series of novel substituted 10-methylacridinium derivatives were designed and synthesized for evaluation of their *in vitro* and *in vivo* antibacterial activity. These compounds were easily accessible in 2−5 synthetic steps with good yields by employing some common intermediates, which constructed the compound library rapidly for the study of antibacterial activity. The results suggested that some compounds of Series A demonstrated moderate antibacterial activity, which compelled us to further design and synthesize Series B, C and D based on the analysis of the SARs to discover better antibacterial agents. As expected, compounds of Series B, C and D exhibited significant antibacterial activity against most of the tested strains, including the multidrug-resistant strains, compared with those of Series A. In addition, some of the above compounds could inhibit the growth of VRE effectively. It is noteworthy that the MIC values of **15f** against susceptible and resistant Gram-positive bacteria ranged from <0.125 to 4 μg/mL, which were much lower than those of lead compound berberine and less than or equal to those observed with antibiotics commonly used in clinical as well. Particularly, **15f** had an MIC value of 4 μg/mL against VRE, which was much lower than that observed for vancomycin (MIC > 64 μg/mL). Considering the fact that **15f** was inactive to Gram-negative bacteria, we further confirmed that **15f** could not inhibit the biofilm formation of *P. aeruginosa* ATCC27853. In bactericidal kinetic assay, **15f** was found to have rapid bactericidal properties, reaching 2.2 log reduction for *S. aureus* ATCC25923 (more than 99.99% of bacteria were killed) within 3 h at 4 × MIC, which demonstrated that **15f** was an excellent bactericidal agent. Its rapid bactericidal activity contributed to overcoming the emergence of drug resistance. Further mechanistic studies by employing various biochemical

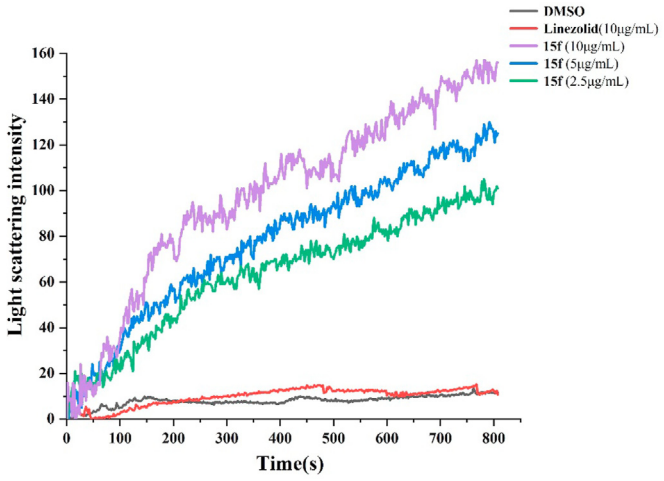

Fig. 7. Time-dependent polymerization profiles of *Bs*FtsZ in the absence and presence of compound **15f** at a concentration range from 2.5 to 10 μg/mL.

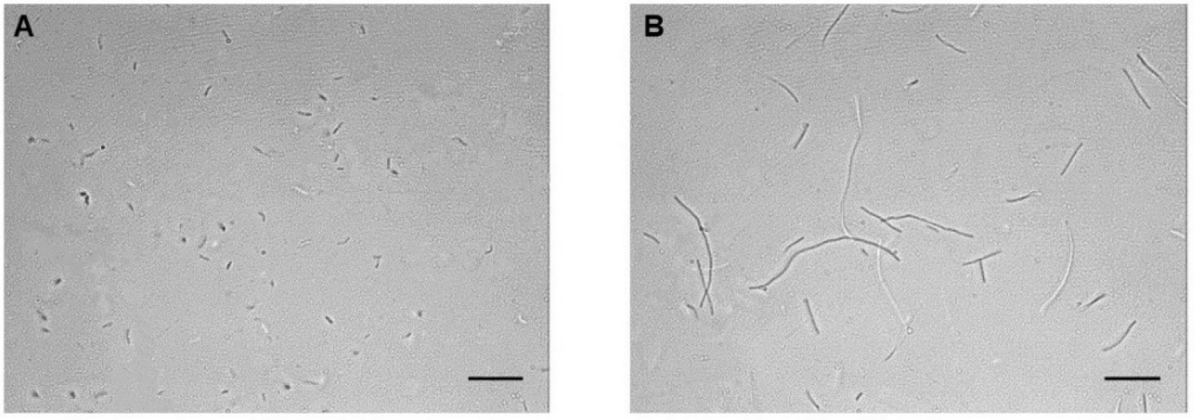

Fig. 6. Effects of compound **15f** on the cell morphology of *B. pumilus* cells in the absence (A) and in the presence (B) of **15f** at 0.25 μg/mL.

assays, microscopic observation and computational docking methods revealed that **15f** functioned as an effective FtsZ inhibitor to stimulate FtsZ polymerization through binding into the inter-domain cleft of FtsZ. In a murine infection model induced by *S. aureus* ATCC25923, **15f** showed an excellent antibacterial efficacy and no significant hemolysis to mammalian cells. Therefore, **15f** can be used as an effective candidate drug for further development to combat drug-resistant pathogen infections.

5. Experimental sections

5.1. General experimental protocol

All commercially available reagents and solvents were used without further purification. Analytical thin-layer chromatography (TLC) was performed on 0.25-mm pre-coated silica GF254 plates and visualized under UV light. Column chromatography of silica gel (200–300 mesh) was used to separate and purify intermediates and compounds. High resolution mass spectra (HRMS) were performed at the Analytical Center for Structural Constituent and Physical Property of Shandong University, Jinan, China. ^{1}H NMR and ^{13}C NMR spectra were recorded on Bruker Avance DRX 400/600 spectrometer (Bruker, Switzerlands) at ambient temperature in $CDCl_3$, DMSO-d_6 or CD_3OD solution. Tetramethylsilane (TMS) was employed as an internal standard of chemical shifts. Melting points were measured using an uncorrected RY-1 melting point apparatus. The high-performance liquid chromatography (HPLC) method was established using an Agilent 1200 Series equipment coupled to ultraviolet–visible detector (UVD) at 254 nm with a Diamonil C_{18} reversed phase column (150 × 4.6 mm, 5 μm), injection volume of 5 μL, and it was maintained at ambient temperature. The effective chromatogram was obtained using the mobile phase of acetonitrile: 0.025 mol/L potassium dihydrogen phosphate buffer (60 : 40, vol/vol) and the pH value was adjusted to 3 with phosphoric acid at the flow rate of 1.0 mL/min. The purity of the test compounds as determined by analytical HPLC was more than 95%.

5.2. Typical procedure for the synthesis of Series A, B, C and D

5.2.1. 2-(Phenylamino)benzoic acid (**2**)

A solution of 2-bromobenzoic acid (2.0 g, 10 mmol), aniline (1.85 g, 20 mmol), Cu powder (0.2–0.3 μm, 4.97 mmol), and K_2CO_3 (1.37g, 10 mmol) in EtOH (80 ml) was heated under reflux for 12 h, monitored by using TLC. The cooled reaction mixture was poured into hot water. The mixture was filtrated through Celite, and then the filtrate was acidified with diluted HCl to pH 5–6. The precipitate was purified using recrystallization from ethanol to obtain pure product as a grey solid (1.65g, 78%). ^{1}H NMR (400 MHz, DMSO-d_6) δ 13.06 (s, 1H), 9.63 (s, 1H), 7.90 (dd, J = 8.0, 1.5 Hz, 1H), 7.37 (ddd, J = 12.8, 9.7, 7.3 Hz, 3H), 7.23 (t, J = 7.5 Hz, 3H), 7.07 (t, J = 7.3 Hz, 1H), 6.78 (t, J = 7.5 Hz, 1H). MS (ESI) m/z calcd for $C_{13}H_{11}NO_2$ $[M - H]^-$, 212.1, found: 212.20.

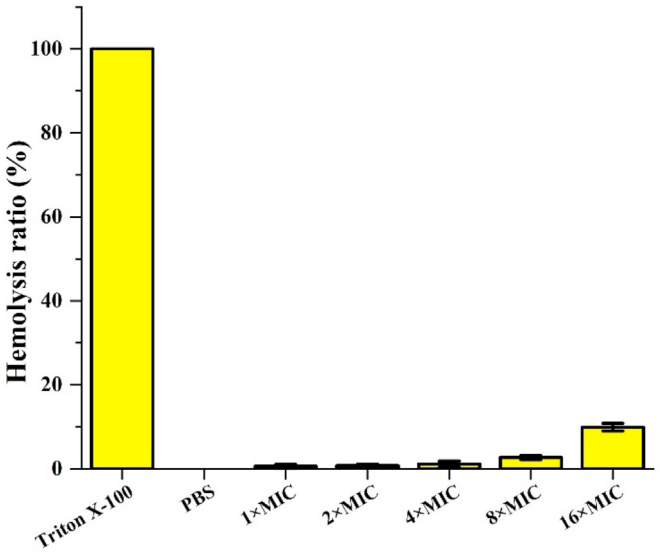

Fig. 9. The hemolysis rate of mice red blood cell induced by positive control (Triton X-100), negative control (PBS) and compound **15f** at 1 × MIC, 2 × MIC, 4 × MIC, 8 × MIC and 16 × MIC, respectively. Bars represent the standard deviation (n = 3).

5.2.2. 9(10H)-Acridinone (**3**)

To a 100 mL round bottom flask containing **2** (2.0 g, 9.4 mmol), was added concentrated H_2SO_4 (10 mL). The mixture was stirred at 100 °C under N_2 atmosphere for 6 h, monitored by using TLC. After cooling down, the reaction mixture was poured into ice water, stirred and filtered. The obtained solid was washed with saturated $NaHCO_3$ solution, and dried to give intermediate **3** as a yellow solid (1.5g, 82%). ^{1}H NMR (400 MHz, DMSO-d_6) δ 11.73 (s, 1H), 8.23 (d, J = 7.8 Hz, 2H), 7.75–7.71 (m, 2H), 7.54 (d, J = 8.3 Hz, 2H), 7.25 (t, J = 7.2 Hz, 2H). MS (ESI) m/z calcd for $C_{13}H_9NO$ $[M + H]^+$, 196.1, found: 391.3.

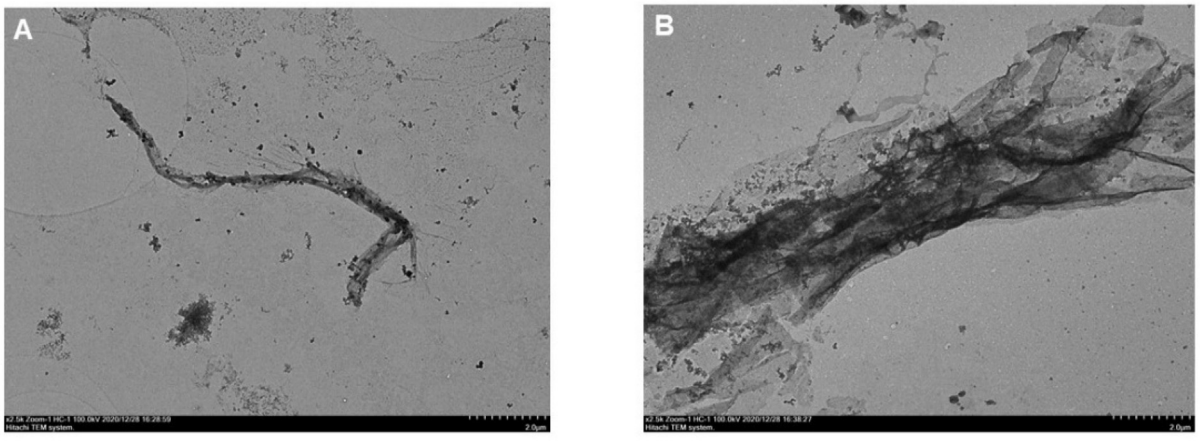

Fig. 8. Transmission electron micrographs of *Bs*FtsZ polymers in the absence (A) and in the presence (B) of **15f** at 10 μg/mL.

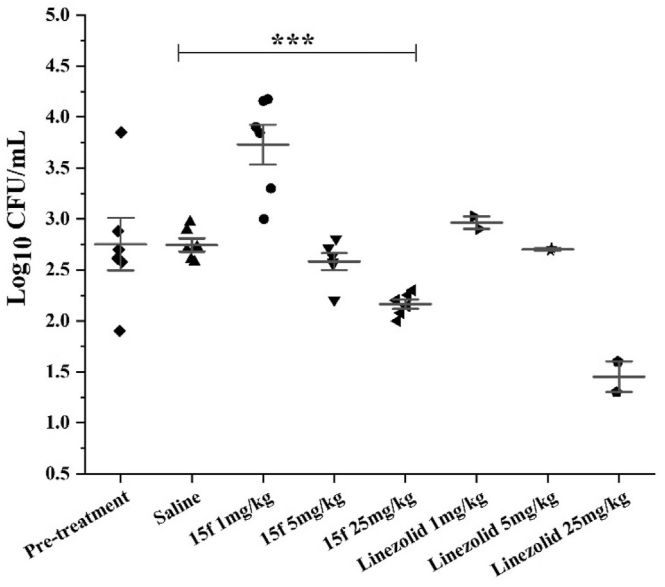

Fig. 10. Efficacy of **15f** in the bacteremia model infected with *S. aureus* ATCC25923. The infected mice were treated with **15f** (1, 5 and 25 mg/kg) or linezolid (1, 5 and 25 mg/kg) via intraperitoneal injection (n = 6). Each point represents the determination of a single animal, and the line shows the mean value. *P < 0.05, **P < 0.01, ***P < 0.001, compared with untreated control group.

*5.2.3. 10-Methylacridin-9(10H)-one (**4**)*

Intermediate **3** (1.5 g, 7.7 mmol) was dissolved in DMF (40 mL) and NaH (65% oil dispersion, 460 mg, 19.2 mmol) was added at 0 °C. The suspension was stirred at 0 °C for 30 min and at 60 °C for 30 min, and then CH_3I (2.7g, 19.2 mmol) was added. The resultant solution was continuously stirred at 60 °C for 18 h. After cooling to room temperature, the reaction solution was quenched with water. The resulting solid was filtrated and dried in vacuo to afford the title compound as a yellow solid (1.4g, 87%). ^{1}H NMR (400 MHz, DMSO-d_6) δ 8.36–8.33 (m, 2H), 7.88–7.81 (m, 4H), 7.34 (ddd, J = 7.9, 6.4, 1.4 Hz, 2H), 3.95 (s, 3H). MS (ESI) m/z calcd for $C_{14}H_{11}NO$ [M + H]$^+$, 210.1, found: 210.3.

*5.2.4. 9-Chloro-10-methylacridin-10-ium chloride (**5**)*

Intermediate **4** (150 mg, 0.57 mmol) was dissolved in $SOCl_2$ (4 mL) and the mixture was refluxed under nitrogen atmosphere for 2 h. After the completion of the reaction, intermediate **5** was obtained as a light yellow solid after concentration under reduced pressure at 50 °C to remove the excess of $SOCl_2$. This intermediate could be used in the next step without purification.

*5.2.5. Typical procedure for the synthesis of Series **A***

A solution of **5** (1.0 eqiv) and substituted amines (1.1eqiv) in anhydrous acetonitrile (7 mL) was heated at 60 °C for 5 h, monitored by using TLC. The reaction mixture was concentrated under reduced pressure and purified on silica gel with DCM/MeOH (20/1) to give the compounds of Series A in good yields.

*5.2.5.1. 10-Methyl-9-(ethylamino)acridin-10-ium chloride. (**6a**).* Yellow solid, yield 82%, m.p.: 240–243 °C; ^{1}H NMR (600 MHz, Chloroform-*d*) δ 12.16 (s, 1H), 9.45 (s, 1H), 8.18 (s, 1H), 7.87 (d, J = 29.9 Hz, 2H), 7.60 (dd, J = 97.0, 77.2 Hz, 4H), 4.05 (s, 3H), 3.48 (s, 2H), 1.73 (t, J = 7.1 Hz, 3H). ^{13}C NMR (150 MHz, $CDCl_3$) δ 159.01, 142.48, 139.65, 135.35, 134.93, 127.52, 127.12, 124.07, 121.98, 116.07, 114.98, 112.09, 44.26, 35.80, 15.20. HRMS (ESI) m/z calcd for $C_{16}H_{17}ClN_2$ [M − Cl]$^+$, 237.1386, found: 237.1395.

*5.2.5.2. 10-Methyl-9-(propylamino)acridin-10-ium chloride. (**6b**).* Yellow solid, yield 78%, m.p.: 200–202 °C; ^{1}H NMR (600 MHz, Chloroform-*d*) δ 12.13 (s, 1H), 9.49 (s, 1H), 8.15 (s, 1H), 7.87 (d, J = 23.7 Hz, 2H), 7.73–7.44 (m, 4H), 4.10–4.07 (m, 2H), 4.05 (s, 3H), 2.25–2.19 (m, 2H), 1.05 (t, J = 7.3 Hz, 3H). ^{13}C NMR (150 MHz, $CDCl_3$) δ 158.77, 135.09, 134.74, 127.13, 126.81, 123.58, 121.61, 115.97, 114.98, 50.64, 35.69, 22.73, 10.89. HRMS (ESI) m/z calcd for $C_{17}H_{19}ClN_2$ [M − Cl]$^+$, 251.1543, found: 251.1550.

*5.2.5.3. 10-Methyl-9-(isopropylamino)acridin-10-ium chloride. (**6c**).* Yellow solid, yield 75%, m.p.: 218–220 °C; ^{1}H NMR (600 MHz, Chloroform-*d*) δ 11.94 (s, 1H), 9.80 (s, 1H), 8.10 (s, 1H), 7.86 (s, 2H), 7.59 (d, J = 83.5 Hz, 4H), 4.67–4.62 (m, 1H), 4.04 (s, 3H), 1.83 (d, J = 6.4 Hz, 6H). ^{13}C NMR (150 MHz, $CDCl_3$) δ 158.80, 135.06, 127.50, 123.98, 121.97, 115.96, 114.89, 52.99, 35.75, 22.77. HRMS (ESI) m/z calcd for $C_{17}H_{19}ClN_2$ [M − Cl]$^+$, 251.1543, found: 251.1559.

*5.2.5.4. 10-Methyl-9-(pentylamino)acridin-10-ium chloride. (**6d**).* Yellow solid, yield 72%, m.p.: 194–197 °C; ^{1}H NMR (600 MHz, Chloroform-*d*) δ 12.12 (s, 1H), 9.45 (s, 1H), 8.16 (s, 1H), 7.86 (d, J = 22.6 Hz, 2H), 7.67 (d, J = 72.4 Hz, 3H), 7.44 (s, 1H), 4.12–4.08 (m,

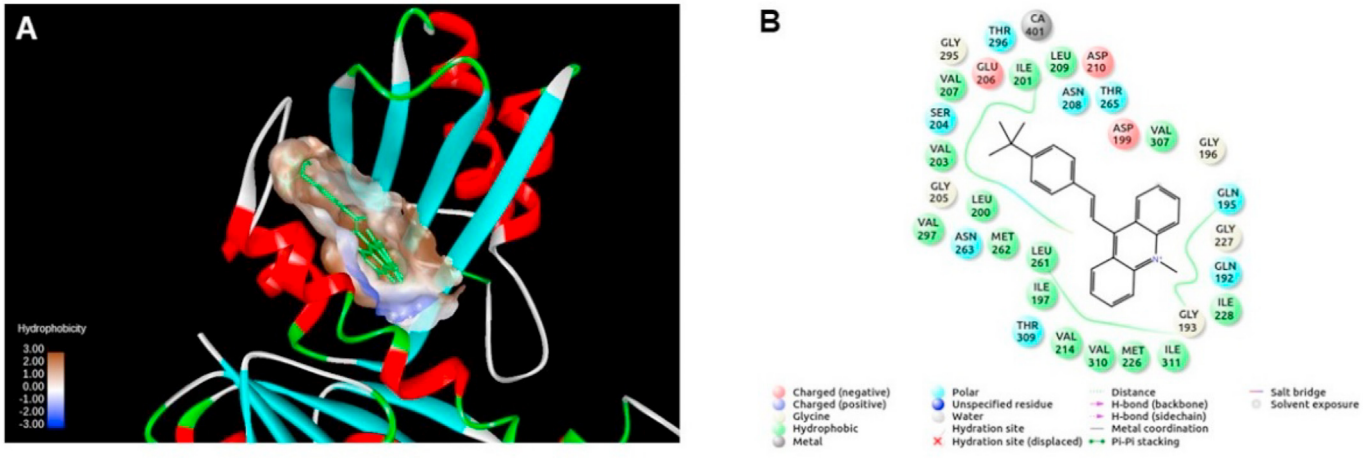

Fig. 11. Predicted binding mode of 10-methylacridinium derivatives. (A) **15f** bound to the C-terminal interdomain cleft of *Sa*FtsZ (PDB: 4DXD); (B) Predicted interaction between **15f** and amino acid residues of *Sa*FtsZ.

2H), 4.04 (s, 3H), 2.20–2.15 (m, 2H), 1.44–1.38 (m, 4H), 0.91 (t, J = 7.0 Hz, 3H). ^{13}C NMR (150 MHz, $CDCl_3$) δ 158.94, 142.47, 139.60, 135.30, 134.84, 127.42, 127.10, 123.94, 121.84, 116.08, 114.99, 112.05, 49.27, 35.79, 29.24, 28.77, 21.98, 13.77. HRMS (ESI) m/z calcd for $C_{19}H_{23}ClN_2$ $[M - Cl]^+$, 279.1856, found: 279.1850.

*5.2.5.5. 10-Methyl-9-(hexylamino)acridin-10-ium chloride. (**6e**).* Yellow solid, yield 74%, m.p.: 188–190 °C; ^{1}H NMR (600 MHz, Chloroform-*d*) δ 12.16 (s, 1H), 9.46 (s, 1H), 8.15 (s, 1H), 7.86 (d, J = 33.1 Hz, 2H), 7.74–7.44 (m, 4H), 4.12–4.08 (m, 2H), 4.04 (s, 3H), 2.18–2.16 (m, 2H), 1.45–1.42 (m, 2H), 1.34–1.31 (m, 4H), 0.86 (t, J = 7.0 Hz, 3H). ^{13}C NMR (150 MHz, $CDCl_3$) δ 158.91, 142.39, 139.58, 135.31, 134.81, 127.38, 127.01, 123.89, 121.82, 116.07, 115.02, 112.03, 49.28, 35.83, 35.80, 30.98, 29.46, 26.30, 22.25, 13.72. HRMS (ESI) m/z calcd for $C_{20}H_{25}ClN_2$ $[M - Cl]^+$, 293.2012, found: 293.2002.

*5.2.5.6. 10-Methyl-9-(heptylamino)acridin-10-ium chloride. (**6f**).* Yellow solid, yield 79%, m.p.: 180–183 °C; ^{1}H NMR (600 MHz, Chloroform-*d*) δ 12.10 (s, 1H), 9.42 (s, 1H), 8.16 (s, 1H), 7.86 (d, J = 22.1 Hz, 2H), 7.72–7.43 (m, 4H), 4.10 (d, J = 8.3 Hz, 2H), 4.04 (s, 3H), 2.18–2.15 (m, 2H), 1.44–1.42 (m, 2H), 1.37–1.34 (m, 2H), 1.28–1.27 (m, 4H), 0.86 (t, J = 6.8 Hz, 3H). ^{13}C NMR (150 MHz, $CDCl_3$) δ 159.08, 142.52, 139.68, 135.28, 134.93, 127.61, 127.28, 124.13, 121.86, 116.04, 114.90, 112.22, 49.40, 35.76, 31.53, 29.62, 28.63, 26.73, 22.38, 13.90. HRMS (ESI) m/z calcd for $C_{21}H_{27}ClN_2$ $[M - Cl]^+$, 307.2169, found: 307.2174.

*5.2.5.7. 10-Methyl-9-(octylamino)acridin-10-ium chloride. (**6g**).* Yellow solid, yield 80%, m.p.: 186–188 °C; ^{1}H NMR (600 MHz, Chloroform-*d*) δ 12.18 (s, 1H), 9.47 (s, 1H), 8.16 (s, 1H), 7.87 (d, J = 23.9 Hz, 2H), 7.73–7.44 (m, 4H), 4.11 (s, 2H), 4.05 (s, 3H), 2.18 (s, 2H), 1.44 (t, J = 7.3 Hz, 2H), 1.36–1.34 (m, 2H), 1.29–1.23 (m, 6H), 0.86 (t, J = 7.0 Hz, 3H). ^{13}C NMR (150 MHz, $CDCl_3$) δ 158.86, 142.35, 139.53, 135.29, 134.78, 127.33, 126.92, 123.84, 121.80, 116.09, 115.04, 111.97, 49.26, 35.84, 31.40, 29.48, 28.85, 28.77, 26.61, 22.27, 13.80. HRMS (ESI) m/z calcd for $C_{22}H_{29}ClN_2$ $[M - Cl]^+$, 321.2325, found: 321.2335.

*5.2.5.8. 10-Methyl-9-(cyclopropylamino)acridin-10-ium chloride. (**6h**).* Yellow solid, yield 78%, m.p.: 220–223 °C; ^{1}H NMR (600 MHz, Chloroform-*d*) δ 12.19 (s, 1H), 8.93 (s, 1H), 7.88 (d, J = 20.4 Hz, 2H), 7.74–7.45 (m, 5H), 4.08 (s, 3H), 3.44–3.40 (m, 1H), 1.57–1.54 (m, 2H), 1.21–1.17 (m, 2H). HRMS (ESI) m/z calcd for $C_{17}H_{17}ClN_2$ $[M - Cl]^+$, 249.1386, found: 249.1395.

*5.2.5.9. 10-Methyl-9-(cyclohexylamino)acridin-10-ium chloride. (**6i**).* Yellow solid, yield 72%, m.p.: 215–219 °C; ^{1}H NMR (600 MHz, Chloroform-*d*) δ 11.75 (s, 1H), 9.77 (s, 1H), 7.86 (s, 2H), 7.65–7.50 (m, 5H), 4.19 (d, J = 9.1 Hz, 1H), 4.03 (s, 3H), 2.73 (d, J = 14.2 Hz, 2H), 2.02 (d, J = 12.8 Hz, 2H), 1.94 (d, J = 13.5 Hz, 2H), 1.66 (d, J = 13.3 Hz, 1H), 1.49–1.46 (m, 1H), 1.27 (d, J = 13.3 Hz, 2H). ^{13}C NMR (150 MHz, $CDCl_3$) δ 158.97, 135.06, 133.73, 127.58, 121.11, 114.69, 60.47, 54.44, 35.67, 32.40, 25.18, 24.28. HRMS (ESI) m/z calcd for $C_{20}H_{23}ClN_2$ $[M - Cl]^+$, 291.1856, found: 291.1856.

*5.2.5.10. 10-Methyl-9-(phenylamino)acridin-10-ium chloride. (**6j**).* Yellow solid, yield 78%, m.p.: 231–235 °C; ^{1}H NMR (600 MHz, Chloroform-*d*) δ 13.57 (s, 1H), 8.76 (s, 3H), 7.73 (d, J = 67.8 Hz, 4H), 7.26 (s, 6H), 4.12 (s, 3H). ^{13}C NMR (150 MHz, $CDCl_3$ + CD_3OD) δ 155.31, 143.53, 141.44, 134.39, 129.45, 127.05, 125.87, 122.47, 122.39, 116.20, 115.58, 35.33. HRMS (ESI) m/z calcd for $C_{20}H_{17}ClN_2$ $[M - Cl]^+$, 285.1386, found: 285.1396.

*5.2.5.11. 10-Methyl-9-((2-ethylphenyl)amino)acridin-10-ium chloride. (**6k**).* Yellow solid, yield 82%, m.p.: 187–191 °C; ^{1}H NMR (600 MHz, Chloroform-*d*) δ 13.49 (s, 1H), 8.76 (s, 2H), 7.83 (d, J = 62.0 Hz, 3H), 7.66 (d, J = 7.7 Hz,1H), 7.40–7.32 (m, 5H), 7.28–7.27 (m, 1H), 4.22 (s, 3H), 2.97–2.94 (m, 2H), 1.36 (t, J = 7.5 Hz, 3H). ^{13}C NMR (150 MHz, $CDCl_3$) δ 156.88, 141.04, 139.27, 137.57, 137.28, 135.87, 129.35, 128.75, 128.64, 128.56, 128.42, 127.30, 127.20, 126.44, 126.38, 123.38, 123.14, 116.83, 114.04, 24.20, 23.40, 13.59, 13.23. HRMS (ESI) m/z calcd for $C_{22}H_{21}ClN_2$ $[M - Cl]^+$, 313.1699, found: 313.1707.

*5.2.5.12. 10-Methyl-9-((2-methoxyphenyl)amino)acridin-10-ium chloride. (**6l**).* Yellow solid, yield 83%, m.p.: 124–128 °C; ^{1}H NMR (600 MHz, Chloroform-*d*) δ 13.38 (s, 1H), 8.90 (s, 2H), 7.83 (d, J = 37.1 Hz, 4H), 7.37 (s, 2H), 7.22 (s, 2H), 6.86 (d, J = 37.4 Hz, 2H), 4.24 (s, 3H), 3.82 (s, 3H). HRMS (ESI) m/z calcd for $C_{21}H_{19}ClN_2$ $[M - Cl]^+$, 315.1492, found: 315.1498.

*5.2.5.13. 10-Methyl-9-((2-(trifluoromethyl)phenyl)amino)acridin-10-ium chloride. (**6m**).* Yellow solid, yield 79%, m.p.: 199–202 °C; ^{1}H NMR (600 MHz, Chloroform-*d*) δ 13.68 (s, 1H), 8.19 (s, 2H), 7.73 (d, J = 35.6 Hz, 4H), 7.56 (d, J = 8.6 Hz, 3H), 7.34 (s, 1H), 7.19 (s, 2H), 4.02 (s, 3H). HRMS (ESI) m/z calcd for $C_{21}H_{16}ClF_3N_2$ $[M - Cl]^+$, 353.1260, found: 353.1266.

*5.2.5.14. 10-Methyl-9-([1,1′-biphenyl]-4-ylamino)acridin-10-ium chloride. (**6n**).* Yellow solid, yield 81%, m.p.: 167–170 °C; ^{1}H NMR (600 MHz, Chloroform-d) δ 7.64 (d, J = 7.4 Hz, 2H), 7.58 (d, J = 8.3 Hz, 3H), 7.53 (d, J = 7.3 Hz, 1H), 7.45–7.38 (m, 6H), 7.33–7.27 (m, 2H), 7.06 (s, 3H), 3.83 (s, 3H). HRMS (ESI) m/z calcd for $C_{26}H_{21}ClN_2$ $[M - Cl]^+$, 361.1699, found: 361.1694.

*5.2.5.15. 10-Methyl-9-((2,4-difluorophenyl)amino)acridin-10-ium chloride. (**6o**).* Yellow solid, yield 84%, m.p.: 254–258 °C; ^{1}H NMR (600 MHz, DMSO-d_6) δ 11.65 (s, 1H), 8.10 (d, J = 115.6 Hz, 6H), 7.38 (d, J = 126.6 Hz, 5H), 4.23 (s, 3H). ^{13}C NMR (150 MHz, CD_3OD + $CDCl_3$) δ 157.85, 142.95, 142.27, 137.20, 134.79, 129.34 (d, $J_{F\text{-}C}$ = 8.6 Hz), 127.02, 125.72, 124.92, 121.79, 118.40, 116.07, 115.16, 113.52 (d, $J_{F\text{-}C}$ = 24.0 Hz), 105.83 (d, $J_{F\text{-}C}$ = 24.0 Hz), 37.57. HRMS (ESI) m/z calcd for $C_{20}H_{15}ClF_2N_2$ $[M - Cl]^+$, 321.1198, found: 321.1207.

*5.2.5.16. 10-Methyl-9-((2,4-dichlorophenyl)amino)acridin-10-ium chloride. (**6p**).* Yellow solid, yield 78%, m.p.: 249–254 °C; ^{1}H NMR (600 MHz, DMSO-d_6) δ 7.77 (d, J = 37.6 Hz, 7H), 7.35 (d, J = 91.4 Hz, 4H), 4.00 (s, 3H). HRMS (ESI) m/z calcd for $C_{20}H_{15}Cl_3N_2$ $[M - Cl]^+$, 353.0607, found: 353.0601.

*5.2.5.17. 10-Methyl-9-((2,4-dimethylphenyl)amino)acridin-10-ium chloride. (**6q**).* Yellow solid, yield 82%, m.p.: 189–192 °C; ^{1}H NMR (600 MHz, Chloroform-*d*) δ 7.83 (d, J = 64.0 Hz, 3H), 7.47 (d, J = 8.0 Hz, 2H), 7.39 (s, 1H), 7.12 (s, 1H), 7.07 (s, 2H), 7.03 (d, J = 7.9 Hz, 2H), 4.21 (s, 3H), 2.52 (s, 6H). HRMS (ESI) m/z calcd for $C_{22}H_{21}ClN_2$ $[M - Cl]^+$, 313.1699, found: 313.1689.

*5.2.5.18. 10-Methyl-9-((2,4-dimethoxyphenyl)amino)acridin-10-ium chloride. (**6r**).* Yellow solid, yield 79%, m.p.: 146–148 °C; ^{1}H NMR (600 MHz, Chloroform-*d*) δ 7.46 (s, 3H), 7.28 (s, 2H), 7.26 (s, 1H), 6.78–6.77 (m, 2H), 6.51–6.46 (m, 3H), 3.82 (s, 3H), 3.71 (s, 3H), 3.62 (s, 3H). ^{13}C NMR (150 MHz, $CDCl_3$ + CD_3OD) δ 155.88, 154.72, 149.72, 134.80, 130.53, 126.80, 119.96, 113.49, 104.58, 99.78, 55.09, 55.04, 33.55. HRMS (ESI) m/z calcd for $C_{22}H_{21}ClN_2O_2$ $[M - Cl]^+$, 345.1598, found: 345.1600.

*5.2.5.19. 10-Methyl-9-(1H-pyrrol-1-yl)acridin-10-ium chloride. (**6s**).* Brown solid, yield 68%, m.p.: 199–203 °C; ^{1}H NMR (600 MHz, DMSO-d_6) δ 8.58 (d, J = 5.0 Hz, 1H), 8.52 (d, J = 5.2 Hz, 2H), 8.34 (dd,

J = 8.0, 1.3 Hz, 2H), 7.87 (d, *J* = 8.4 Hz, 2H), 7.85–7.82 (m, 2H), 7.36–7.33 (m, 2H), 6.88 (t, *J* = 5.2 Hz, 1H), 3.95 (s, 3H). ^{13}C NMR (150 MHz, CD_3OD) δ 152.88, 142.40, 138.37, 131.48, 127.71, 126.58, 125.70, 123.92, 120.33, 120.30, 118.70, 111.97, 38.40. HRMS (ESI) *m*/*z* calcd for $C_{18}H_{15}ClN_2$ $[M - Cl]^+$, 259.1230, found: 259.1228.

*5.2.5.20. 10-Methyl-9-(thiazol-2-ylamino)acridin-10-ium chloride. (**6t**).* Dark red solid, yield 69%, m.p.: 137–141 °C; ^{1}H NMR (600 MHz, Chloroform-*d*) δ 8.14–8.13 (m, 2H), 7.64 (t, *J* = 7.5 Hz, 2H), 7.47 (d, *J* = 8.2 Hz, 3H), 7.14 (t, *J* = 7.5 Hz, 2H), 6.90–6.89 (m, 1H), 3.89 (s, 3H), 3.49 (s, 1H). ^{13}C NMR (150 MHz, $CDCl_3$ + CD_3OD) δ 158.09, 141.55, 133.68, 132.43, 127.85, 127.17, 121.03, 120.86, 119.16, 114.60, 114.48, 34.14. HRMS (ESI) *m*/*z* calcd for $C_{17}H_{14}ClN_3S$ $[M - Cl]^+$, 292.0903, found: 292.0893.

*5.2.5.21. 10-Methyl-9-(pyridin-2-ylamino)acridin-10-ium chloride. (**6u**).* Yellow solid, yield 72%, m.p.: 188–191 °C; ^{1}H NMR (600 MHz, Chloroform-*d*) δ 8.57 (dd, *J* = 8.0, 1.7 Hz, 2H), 7.85 (d, *J* = 5.4 Hz, 1H), 7.74 (ddd, *J* = 8.7, 7.0, 1.7 Hz, 2H), 7.61–7.58 (m, 2H), 7.55 (d, *J* = 8.7 Hz, 2H), 7.31 (t, *J* = 7.5 Hz, 2H), 6.85 (d, *J* = 8.7 Hz, 1H), 6.70 (t, *J* = 6.4 Hz, 1H), 3.92 (s, 3H). ^{13}C NMR (150 MHz, $CDCl_3$ + CD_3OD) δ 177.94, 155.94, 142.03, 140.60, 139.77, 133.61, 132.27, 127.53, 126.93, 121.70, 120.94, 114.57, 112.37, 111.52, 33.23. HRMS (ESI) *m*/*z* calcd for $C_{19}H_{16}ClN_3$ $[M - Cl]^+$, 286.1339, found: 286.1338.

*5.2.5.22. 10-Methyl-9-(pyrimidin-2-ylamino)acridin-10-ium chloride. (**6v**).* Orange solid, yield 71%, m.p.: 179–183 °C; ^{1}H NMR (600 MHz, DMSO-d_6) δ 12.42 (s, 1H), 8.74 (d, *J* = 9.1 Hz, 2H), 8.51 (dd, *J* = 8.7, 1.1 Hz, 2H), 8.40–8.37 (m, 2H), 7.96 (dd, *J* = 8.3, 7.1 Hz, 2H), 7.60–7.59 (m, 1H), 6.96 (t, *J* = 3.6 Hz, 1H), 6.66–6.49 (m, 1H), 4.79 (s, 3H). HRMS (ESI) *m*/*z* calcd for $C_{18}H_{15}ClN_4$ $[M - Cl]^+$, 287.1291, found: 287.1280.

*5.2.5.23. 10-Methyl-9-(pyrimidin-4-ylamino)acridin-10-ium chloride. (**6w**).* Yellow solid, yield 70%, m.p.: 191–194 °C; ^{1}H NMR (600 MHz, Chloroform-*d*) δ 8.82 (s, 1H), 8.36 (d, *J* = 5.6 Hz, 1H), 8.03 (d, *J* = 7.3 Hz, 2H), 7.68 (t, *J* = 7.6 Hz, 2H), 7.52 (d, *J* = 8.4 Hz, 2H), 7.18 (t, *J* = 7.3 Hz, 2H), 6.71 (s, 1H), 3.93 (s, 3H). ^{13}C NMR (150 MHz, $CDCl_3$) δ 159.42, 156.43, 141.75, 132.44, 128.30, 121.03, 119.42, 114.50, 111.10, 34.24. HRMS (ESI) *m*/*z* calcd for $C_{18}H_{15}ClN_4$ $[M - Cl]^+$, 287.1291, found: 287.1289.

*5.2.6. 9-Bromoacridine (**7**)*

PBr_3 (19.5 mL, 205 mmol) was added dropwise to a 250 mL round bottom flask containing **3** (4.0 g, 20.5 mmol) at 0 °C under N_2 atmosphere. After stirring at 110 °C for 24 h, the resultant solution was quenched by slow addition of H_2O and an aqueous NaOH solution was added to the resultant mixture until pH = 14. The crude product was extracted with CH_2Cl_2 (50 mL × 3). The combined organic extracts were washed with brine, dried over Na_2SO_4, filtrated, and concentrated under reduced pressure to obtain the title compound as a yellow solid (3.81 g, 72%). ^{1}H NMR (400 MHz, Chloroform-*d*) δ 8.45 (d, *J* = 8.8 Hz, 2H), 8.27 (d, *J* = 8.6 Hz, 2H), 7.85–7.81 (m, 2H), 7.69–7.65 (m, 2H). MS (ESI) *m*/*z* calcd for $C_{13}H_8BrN$ $[M + H]^+$, 258.0, found: 260.2.

*5.2.7. 9-(3-Methoxyphenyl)acridine (**8d**)*

To a solution of **7** (150 mg, 0.58 mmol) in dioxane and water (5:1), aryl boronic acid (0.11 g, 0.87 mmol), and K_2CO_3 (0.24 g, 17.4 mmol) was added under N_2 atmosphere. After $Pd(PPh_3)_4$ (0.005 mmol) was added, the resulting solution was heated to 100 °C for 8 h. After completion of the reaction, the aqueous layer was extracted with CH_2Cl_2 (30 mL × 3). The combined organic layer was dried over Na_2SO_4, filtrated, concentrated under reduced pressure and the residue was purified on silica gel with petroleum ether/EtOAc (8/1) to give titled compound (0.13 g) as a white solid in 89% yield. ^{1}H NMR (400 MHz, Chloroform-*d*) δ 8.31 (d, *J* = 8.2 Hz, 2H), 7.77 (dd, *J* = 18.2, 8.0 Hz, 4H), 7.54–7.50 (m, 1H), 7.47–7.43 (m, 2H), 7.13 (dd, *J* = 8.2, 2.2 Hz, 1H), 7.03 (d, *J* = 7.5 Hz, 1H), 6.99 (d, *J* = 2.0 Hz, 1H), 3.87 (s, 3H). MS (ESI) *m*/*z* calcd for $C_{20}H_{15}NO$ $[M + H]^+$, 287.1, found: 287.6.

*5.2.8. Typical procedure for the synthesis of Series **B***

Intermediate **8d** (100 mg, 0.39 mmol) was dissolved in an excess of CH_3I (0.25 mL, 3.9 mmol) within a sealed tube. The mixture was heated at 85 °C for 24 h and then isopropyl ether (50 mL) was added to separate out a dark red solid. The crude product was purified via column chromatography (DCM/MeOH 10/1) to yield the corresponding product as a red solid (80 mg, 76%).

*5.2.8.1. 10-Methyl-9-phenylacridin-10-ium iodide. (**9a**).* Red solid, yield 76%, m.p.: 236–240 °C; ^{1}H NMR (600 MHz, Chloroform-*d*) δ 8.94 (d, *J* = 9.2 Hz, 2H), 8.42 (ddd, *J* = 9.0, 6.7, 1.3 Hz, 2H), 8.01 (dd, *J* = 8.7, 1.1 Hz, 2H), 7.81 (dd, *J* = 8.5, 6.8 Hz, 2H), 7.75–7.71 (m, 3H), 7.50–7.49 (m, 2H), 5.28 (s, 3H). ^{13}C NMR (150 MHz, $CDCl_3$) δ 160.78, 140.86, 138.94, 132.26, 130.02, 129.63, 129.23, 128.54, 127.58, 125.51, 118.92, 40.80. HRMS (ESI) *m*/*z* calcd for $C_{20}H_{16}IN$ $[M - I]^+$, 270.1277, found: 270.1279.

*5.2.8.2. 10-Methyl-9-(o-tolyl)acridin-10-ium iodide. (**9b**).* Red solid, yield 72%, m.p.: 230–233 °C; ^{1}H NMR (600 MHz, Chloroform-*d*) δ 8.97 (d, *J* = 9.2 Hz, 2H), 8.44–8.41 (m, 2H), 7.88–7.86 (m, 2H), 7.80 (dd, *J* = 8.5, 6.7 Hz, 2H), 7.65–7.62 (m, 1H), 7.55–7.50 (m, 2H), 7.27 (s, 1H), 5.30 (s, 1H), 1.93 (s, 1H). ^{13}C NMR (150 MHz, $CDCl_3$) δ 161.44, 141.16, 139.35, 135.88, 132.30, 130.70, 130.35, 129.36, 129.10, 128.10, 126.18, 125.75, 119.57, 41.22, 19.80. HRMS (ESI) *m*/*z* calcd for $C_{21}H_{18}IN$ $[M - I]^+$, 284.1434, found: 284.1428.

*5.2.8.3. 10-Methyl-9-(m-tolyl)acridin-10-ium iodide. (**9c**).* Red solid, yield 69%, m.p.: 226–228 °C; ^{1}H NMR (600 MHz, Chloroform-*d*) δ 8.95 (d, *J* = 9.2 Hz, 2H), 8.42 (ddd, *J* = 9.0, 6.7, 1.3 Hz, 2H), 8.02 (dd, *J* = 8.7, 1.1 Hz, 2H), 7.81 (dd, *J* = 8.5, 6.8 Hz, 2H), 7.59 (t, *J* = 7.9 Hz, 1H), 7.53 (d, *J* = 7.6 Hz, 1H), 7.27 (d, *J* = 7.1 Hz, 2H), 5.27 (s, 3H), 2.53 (s, 3H). ^{13}C NMR (150 MHz, $CDCl_3$) δ 161.42, 141.14, 139.14, 138.74, 132.56, 130.99, 130.04, 129.92, 128.65, 127.73, 126.69, 125.80, 119.20, 41.11, 21.29. HRMS (ESI) *m*/*z* calcd for $C_{21}H_{18}IN$ $[M - I]^+$, 284.1434, found: 284.1442.

*5.2.8.4. 10-Methyl-9-(3-methoxyphenyl)acridin-10-ium iodide. (**9d**).* Red solid, yield 70%, m.p.: 227–229 °C; ^{1}H NMR (600 MHz, Chloroform-*d*) δ 8.94 (dd, *J* = 9.2, 3.6 Hz, 2H), 8.43–8.40 (m, 2H), 8.05–8.03 (m, 2H), 7.82–7.80 (m, 2H), 7.63–7.60 (m, 1H), 7.25–7.23 (m, 1H), 7.05 (dd, *J* = 7.4, 1.3 Hz, 1H), 7.02–7.01 (m, 1H), 5.26 (s, 3H), 3.89 (s, 3H). ^{13}C NMR (150 MHz, $CDCl_3$) δ 160.62, 159.24, 140.99, 139.08, 133.64, 129.95, 129.79, 127.70, 125.59, 121.67, 119.05, 115.35, 115.20, 55.38, 40.96. HRMS (ESI) *m*/*z* calcd for $C_{21}H_{18}INO$ $[M - I]^+$, 300.1383, found: 300.1373.

*5.2.8.5. 10-Methyl-9-(3-fluorophenyl)acridin-10-ium iodide. (**9e**).* Red solid, yield 68%, m.p.: 230–232 °C; ^{1}H NMR (600 MHz, Chloroform-*d*) δ 8.95 (d, *J* = 9.2 Hz, 2H), 8.43 (ddd, *J* = 8.9, 6.7, 1.5 Hz, 2H), 7.98 (d, *J* = 8.6 Hz, 2H), 7.85–7.83 (m, 2H), 7.74–7.70 (m, 1H), 7.47–7.44 (m, 1H), 7.32 (d, *J* = 7.5 Hz, 1H), 7.24 (t, *J* = 2.1 Hz, 1H), 5.28 (s, 3H). ^{13}C NMR (150 MHz, $CDCl_3$) δ 163.19, 161.52, 158.85 (d, $J_{F\text{-}C}$ = 2.0 Hz), 141.34, 139.31, 134.62 (d, $J_{F\text{-}C}$ = 7.7 Hz), 131.04 (d, $J_{F\text{-}C}$ = 8.3 Hz), 129.49, 128.16, 125.78, 125.56 (d, $J_{F\text{-}C}$ = 3.3 Hz), 119.59, 117.45 (d, $J_{F\text{-}C}$ = 20.9 Hz), 116.88 (d, $J_{F\text{-}C}$ = 23.2 Hz), 41.45. HRMS (ESI) *m*/*z* calcd for $C_{20}H_{15}FIN$ $[M - I]^+$, 288.1183, found: 288.1196.

*5.2.8.6. 10-Methyl-9-(3-nitrophenyl)acridin-10-ium iodide. (**9f**).* Red solid, yield 72%, m.p.: 232–236 °C; ^{1}H NMR (600 MHz, Chloroform-*d*) δ 8.92 (d, *J* = 9.2 Hz, 2H), 8.62 (d, *J* = 7.9 Hz, 1H), 8.44 (ddd, *J* = 8.5, 6.1, 1.7 Hz, 2H), 8.39 (s, 1H), 8.01–7.97 (m, 2H), 7.89–7.86 (m, 4H), 5.27 (s, 3H). ^{13}C NMR (150 MHz, DMSO) δ 157.35, 147.64, 140.82, 138.26, 135.81, 134.25, 130.38, 129.12, 127.86, 125.29, 124.57, 124.44, 118.93. HRMS (ESI) *m*/*z* calcd for $C_{20}H_{15}IN_2O_2$ $[M - I]^+$, 315.1128, found: 315.1138.

*5.2.8.7. 10-Methyl-9-(p-tolyl)acridin-10-ium iodide. (**9g**).* Red solid, yield 71%, m.p.: 240–242 °C; ^{1}H NMR (600 MHz, Chloroform-*d*) δ 8.93 (d, *J* = 9.1 Hz, 2H), 8.42–8.40 (m, 2H), 8.05 (d, *J* = 8.6 Hz, 2H), 7.81–7.79 (m, 2H), 7.52 (d, *J* = 7.7 Hz, 2H), 7.38 (d, *J* = 7.8 Hz, 2H), 5.26 (s, 3H), 2.58 (s, 3H). ^{13}C NMR (150 MHz, $CDCl_3$) δ 161.51, 141.05, 140.59, 139.04, 129.97, 129.53, 129.46, 129.37, 127.62, 125.80, 119.08, 40.97, 21.24. HRMS (ESI) *m*/*z* calcd for $C_{21}H_{18}IN$ $[M - I]^+$, 284.1434, found: 284.1449.

*5.2.8.8. 10-Methyl-9-(4-ethylphenyl)acridin-10-ium iodide. (**9h**).* Red solid, yield 66%, m.p.: 240–242 °C; ^{1}H NMR (600 MHz, Chloroform-d) δ 8.94 (d, *J* = 9.2 Hz, 2H), 8.43–8.40 (m, 2H), 8.05 (dd, *J* = 8.7, 1.1 Hz, 2H), 7.80 (dd, *J* = 8.4, 6.9 Hz, 2H), 7.54 (d, *J* = 7.9 Hz, 2H), 7.40 (d, *J* = 8.0 Hz, 2H), 5.26 (s, 3H), 2.90–2.86 (m, 2H), 1.41 (t, *J* = 7.6 Hz, 3H). ^{13}C NMR (150 MHz, $CDCl_3$) δ 161.42, 146.61, 140.94, 138.96, 129.91, 129.57, 129.55, 128.08, 127.54, 125.70, 118.97, 40.86, 28.36, 14.94. HRMS (ESI) *m*/*z* calcd for $C_{22}H_{20}IN$ $[M - I]^+$, 298.1590, found: 298.1590.

*5.2.8.9. 10-Methyl-9-(4-propylphenyl)acridin-10-ium iodide. (**9i**).* Red solid, yield 74%, m.p.: 230–232 °C; ^{1}H NMR (600 MHz, Chloroform-*d*) δ 8.94 (d, *J* = 9.2 Hz, 2H), 8.42 (ddd, *J* = 9.0, 6.7, 1.3 Hz, 2H), 8.05 (dd, *J* = 8.7, 1.1 Hz, 2H), 7.80 (dd, *J* = 8.5, 6.8 Hz, 2H), 7.52 (d, *J* = 7.9 Hz, 2H), 7.39 (d, *J* = 8.0 Hz, 2H), 5.26 (s, 3H), 2.82–2.79 (m, 2H), 1.84–1.78 (m, 2H), 1.07 (t, *J* = 7.3 Hz, 3H). ^{13}C NMR (150 MHz, $CDCl_3$) δ 161.51, 145.26, 141.06, 139.04, 129.99, 129.71, 129.57, 128.73, 127.62, 125.80, 119.10, 41.00, 37.55, 24.05, 13.63. HRMS (ESI) *m*/*z* calcd for $C_{23}H_{22}IN$ $[M - I]^+$, 312.1747, found: 312.1751.

*5.2.8.10. 10-Methyl-9-(4-butylphenyl)acridin-10-ium iodide. (**9j**).* Red solid, yield 73%, m.p.: 190–194 °C; ^{1}H NMR (600 MHz, Chloroform-*d*) δ 8.94 (d, *J* = 9.2 Hz, 2H), 8.42 (ddd, *J* = 9.0, 6.7, 1.3 Hz, 2H), 8.06–8.04 (m, 2H), 7.80 (dd, *J* = 8.4, 6.9 Hz, 2H), 7.52 (d, *J* = 8.0 Hz, 2H), 7.39 (d, *J* = 8.0 Hz, 2H), 5.26 (s, 3H), 2.84–2.81 (m, 2H), 1.79–1.74 (m, 2H), 1.52–1.45 (m, 2H), 1.02 (t, *J* = 7.4 Hz, 3H). ^{13}C NMR (150 MHz, $CDCl_3$) δ 161.36, 145.31, 140.88, 138.91, 129.84, 129.50, 129.44, 128.52, 127.50, 125.63, 118.91, 40.79, 35.06, 32.91, 21.96, 13.54. HRMS (ESI) *m*/*z* calcd for $C_{24}H_{24}IN$ $[M - I]^+$, 326.1903, found: 326.1913.

*5.2.8.11. 10-Methyl-9-(4-methoxyphenyl)acridin-10-ium iodide. (**9k**).* Red solid, yield 69%, m.p.: 248–250 °C; ^{1}H NMR (600 MHz, Chloroform-*d*) δ 8.91 (d, *J* = 9.2 Hz, 2H), 8.41 (ddd, *J* = 9.0, 6.7, 1.4 Hz, 2H), 8.11–8.09 (m, 2H), 7.82–7.80 (m, 2H), 7.45–7.43 (m, 2H), 7.23 (d, *J* = 8.7 Hz, 2H), 5.23 (s, 3H), 3.99 (s, 3H). ^{13}C NMR (150 MHz, $CDCl_3$) δ 161.29, 160.99, 141.00, 138.90, 131.40, 130.00, 127.54, 125.84, 124.19, 118.95, 114.26, 55.47, 40.80. HRMS (ESI) *m*/*z* calcd for $C_{21}H_{18}INO$ $[M - I]^+$, 300.1383, found: 300.1382.

*5.2.8.12. 10-Methyl-9-([1,1′-biphenyl]-4-yl)acridin-10-ium iodide. (**9l**).* Red solid, yield 77%, m.p.: 230–232 °C; ^{1}H NMR (600 MHz, Chloroform-*d*) δ 8.95 (d, *J* = 9.2 Hz, 2H), 8.43 (ddd, *J* = 9.0, 6.7, 1.3 Hz, 2H), 8.13–8.11 (m, 2H), 7.94 (d, *J* = 8.1 Hz, 2H), 7.85–7.82 (m, 2H), 7.76–7.75 (m, 2H), 7.60–7.55 (m, 4H), 7.48 (t, *J* = 7.4 Hz, 1H), 5.28 (s, 3H). ^{13}C NMR (150 MHz, DMSO) δ 159.82, 141.29, 140.79, 138.57, 138.07, 131.74, 130.29, 129.21, 128.80, 127.84, 127.60, 126.65, 126.55, 125.17, 118.93. HRMS (ESI) *m*/*z* calcd for $C_{26}H_{20}IN$ $[M - I]^+$, 346.1590, found: 346.1583.

*5.2.8.13. 10-Methyl-9-(4-(trifluoromethyl)phenyl)acridin-10-ium iodide. (**9m**).* Red solid, yield 71%, m.p.: 241–246 °C; ^{1}H NMR (600 MHz, Chloroform-*d*) δ 8.97 (d, *J* = 9.2 Hz, 2H), 8.44 (ddd, *J* = 9.0, 6.7, 1.4 Hz, 2H), 8.00 (d, *J* = 8.0 Hz, 2H), 7.90–7.89 (m, 2H), 7.85–7.82 (m, 2H), 7.70 (d, *J* = 7.9 Hz, 2H), 5.28 (s, 3H). ^{13}C NMR (150 MHz, $CDCl_3$) δ 158.53, 141.13, 139.20, 136.37, 132.04 (q, $J_{F\text{-}C}$ = 33.1 Hz), 130.02, 129.15, 128.13, 125.72 (q, $J_{F\text{-}C}$ = 3.7 Hz), 125.59, 124.13, 122.32, 119.40, 41.21. HRMS (ESI) *m*/*z* calcd for $C_{21}H_{15}F_3IN$ $[M - I]^+$, 338.1151, found: 338.1163.

*5.2.8.14. 10-Methyl-9-(4-(trifluoromethoxy)phenyl)acridin-10-ium iodide. (**9n**).* Red solid, yield 67%, m.p.: 204–208 °C; ^{1}H NMR (600 MHz, Chloroform-*d*) δ 8.95 (d, *J* = 9.2 Hz, 2H), 8.43 (ddd, *J* = 9.0, 6.7, 1.3 Hz, 2H), 8.00–7.95 (m, 2H), 7.85–7.83 (m, 2H), 7.61–7.57 (m, 4H), 5.27 (s, 3H). ^{13}C NMR (150 MHz, $CDCl_3$) δ 158.98, 150.23 (d, $J_{F\text{-}C}$ = 2.1 Hz), 141.12, 139.13, 131.34, 130.98, 129.33, 128.02, 125.78, 120.98, 119.33, 41.15. HRMS (ESI) *m*/*z* calcd for $C_{21}H_{15}F_3INO$ $[M - I]^+$, 354.1100, found: 354.1117.

*5.2.8.15. 10-Methyl-9-(4-formylphenyl)acridin-10-ium iodide. (**9o**).* Red solid, yield 69%, m.p.: 246–248 °C; ^{1}H NMR (600 MHz, Chloroform-*d*) δ 10.26 (s, 1H), 8.95 (d, *J* = 9.2 Hz, 2H), 8.45–8.42 (m, 2H), 8.25 (d, *J* = 7.8 Hz, 2H), 7.91 (d, *J* = 8.4 Hz, 2H), 7.83 (dd, *J* = 8.7, 6.6 Hz, 2H), 7.74 (d, *J* = 7.9 Hz, 2H), 5.28 (s, 3H). ^{13}C NMR (150 MHz, DMSO + CD_3OD) δ 192.68, 158.82, 141.08, 138.78, 138.37, 136.88, 130.53, 129.55, 129.10, 127.94, 125.16, 119.13. HRMS (ESI) *m*/*z* calcd for $C_{21}H_{16}INO$ $[M - I]^+$, 298.1226, found: 298.1229.

*5.2.9. 9-Methylacridine (**11**)*

A mixture of *N*,*N*-diphenylamine (3.0g, 17.7 mmol), AcOH (3.2 g, 53.2 mmol), and $ZnCl_2$ (12.0 g, 88.6 mmol) was heated with efficient stirring. When the temperature reached to 180 °C, the excess AcOH was removed from the reaction mixture by distillation. Then, the reaction mixture was heated at 220 °C for additional 5 h under stirring. After the addition of aqueous ammonia solution, the yellow precipitates were obtained by filtration and subsequently dissolved in CH_2Cl_2. The CH_2Cl_2 solution was neutralized by washing with aqueous $NaHCO_3$ and brine, dried over Na_2SO_4, filtrated, concentrated under reduced pressure. The residue was purified on silica gel with petroleum ether/EtOAc (5/1), yielding the pale yellow solid (2.77 g, 81%). ^{1}H NMR (400 MHz, Chloroform-*d*) δ 8.24 (dd, *J* = 12.0, 8.9 Hz, 4H), 7.79–7.75 (m, 2H), 7.58–7.54 (m, 2H), 3.13 (s, 3H). MS (ESI) *m*/*z* calcd for $C_{14}H_{11}N$ $[M + H]^+$, 194.1, found: 194.4.

*5.2.10. 9-(Bromomethyl)acridine (**12**)*

To a solution of **11** (2.0 g, 10.4 mmol) in CCl_4 (100 mL) was added AIBN (0.17 g, 1.0 mmol) and heated to 60 °C under stirring for 30 min. Then NBS (0.17 g, 11.4 mmol) was added and the reaction mixture was heated under refluxing conditions for 4 h. After completion of the reaction, the reaction solution was diluted with CH_2Cl_2. The organic layer was separated, dried over Na_2SO_4, filtrated, and concentrated under reduced pressure. The residue was purified by silica gel using petroleum ether/EtOAc (5/1) as eluent to afford intermediate **12** (2.45 g) in 87% yield. ^{1}H NMR (400 MHz, DMSO-d_6) δ 8.85 (d, *J* = 8.8 Hz, 1H), 8.29 (d, *J* = 8.6 Hz, 4H), 7.98–7.94 (m, 2H), 7.80 (d, *J* = 7.7 Hz, 1H), 5.89 (s, 2H). MS (ESI) *m*/*z* calcd for $C_{14}H_{10}BrN$ $[M + H]^+$, 272.0, found: 274.3.

*5.2.11. Diethyl (acridin-9-ylmethyl)phosphonate (**13**)*

The mixture of **12** (1.0 g, 3.7 mmol) and triethyl phosphite (4 mL) was heated to reflux for 4 h. After cooling down to room temperature, the excess triethyl phosphite was removed under reduced

pressure to afford intermediate **13** (1.1 g) in a 92% yield.

*5.2.12. (E)-9-styrylacridine (**14a**)*

To a solution of **13** (0.15 g, 0.45 mmol) and benzaldehyde (0.05 g, 0.45 mmol) in dry THF (25 mL), NaH (65% oil dispersion, 33.5 mg, 0.9 mmol) was added carefully in an ice-water bath. After the completion of the addition, the solution mixture was warmed to room temperature and stirred overnight. After quenching by water, the resulting mixture was extracted with EtOAc (50 mL × 3). The combined organic layer was washed with brine, dried over Na_2SO_4, filtrated, and concentrated under reduced pressure. The resulting crude product was purified by silica gel using DCM/MeOH (60/1) to afford **14a** (85 mg) in a 67% yield.

*5.2.13. Typical procedure for the synthesis of Series **C***

The titled compound **15a** (66 mg, 74%) were prepared from **14a** (85 mg, 0.3 mmol) and CH_3I (0.43 g, 3.0 mmol) according to the preparation procedure of **9d** described above.

*5.2.13.1. (E)-10-methyl-9-styrylacridin-10-ium iodide. (**15a**).* Dark red solid, yield 76%, m.p.: 200–204 °C; ^{1}H NMR (600 MHz, Chloroform-*d*) δ 8.84 (d, *J* = 9.2 Hz, 2H), 8.70 (d, *J* = 7.8 Hz, 2H), 8.41 (ddd, *J* = 9.2, 6.6, 1.4 Hz, 2H), 8.12 (d, *J* = 16.4 Hz, 1H), 7.92–7.89 (m, 2H), 7.79–7.77 (m, 2H), 7.56–7.51 (m, 3H), 7.23 (d, *J* = 16.4 Hz, 1H), 5.14 (s, 3H). ^{13}C NMR (150 MHz, $CDCl_3$) δ 157.78, 146.11, 140.88, 138.91, 134.60, 130.59, 129.10, 128.91, 127.95, 127.66, 124.75, 119.69, 119.15, 40.80. HRMS (ESI) *m*/*z* calcd for $C_{22}H_{18}IN$ $[M - I]^+$, 296.1434, found: 296.1438.

*5.2.13.2. (E)-10-methyl-9-(2-methoxystyryl)acridin-10-ium iodide. (**15b**).* Dark red solid, yield 69%, m.p.: 184–187 °C; ^{1}H NMR (600 MHz, Chloroform-*d*) δ 8.84 (s, 2H), 8.71 (d, *J* = 8.2 Hz, 2H), 8.40 (s, 2H), 8.26 (d, *J* = 16.1 Hz, 1H), 7.89 (s, 2H), 7.78 (d, *J* = 7.2 Hz, 1H), 7.51–7.47 (m, 2H), 7.13 (t, *J* = 7.3 Hz, 1H), 7.05 (d, *J* = 8.4 Hz, 1H), 5.14 (s, 3H), 3.96 (s, 3H). ^{13}C NMR (150 MHz, DMSO + $CDCl_3$) δ 157.63, 157.22, 140.48, 140.35, 137.63, 131.58, 128.52, 127.81, 126.90, 123.85, 123.42, 120.75, 120.37, 118.64, 111.35, 55.40. HRMS (ESI) *m*/*z* calcd for $C_{23}H_{20}INO$ $[M - I]^+$, 326.1539, found: 326.1532.

*5.2.13.3. (E)-10-methyl-9-(4-methylstyryl)acridin-10-ium iodide. (**15c**).* Brown solid, yield 77%, m.p.: 250–253 °C; ^{1}H NMR (600 MHz, DMSO-d_6) δ 8.85 (d, *J* = 9.6 Hz, 2H), 8.75 (d, *J* = 9.2 Hz, 2H), 8.55 (d, *J* = 16.4 Hz, 1H), 8.44–8.42 (m, 2H), 8.00–7.98 (m, 2H), 7.90 (d, *J* = 8.1 Hz, 2H), 7.37 (d, *J* = 7.9 Hz, 2H), 7.31 (d, *J* = 16.3 Hz, 1H), 4.81 (s, 3H), 2.41 (s, 3H). ^{13}C NMR (150 MHz, DMSO) δ 157.52, 145.78, 140.53, 140.01, 137.72, 132.55, 129.20, 128.73, 128.07, 126.96, 123.92, 119.65, 118.69, 54.57, 48.21, 20.76. HRMS (ESI) *m*/*z* calcd for $C_{23}H_{20}IN$ $[M - I]^+$, 310.1590, found: 310.1604.

*5.2.13.4. (E)-10-methyl-9-(4-ethylstyryl)acridin-10-ium iodide. (**15d**).* Brown solid, yield 72%, m.p.: 222–226 °C; ^{1}H NMR (600 MHz, Chloroform-*d*) δ 8.82 (d, *J* = 8.5 Hz, 2H), 8.69 (d, *J* = 8.5 Hz, 2H), 8.39 (t, *J* = 7.1 Hz, 2H), 8.10 (d, *J* = 16.2 Hz, 1H), 7.90–7.87 (m, 2H), 7.71 (d, *J* = 7.9 Hz, 2H), 7.37 (d, *J* = 7.7 Hz, 2H), 7.22 (d, *J* = 16.2 Hz, 1H), 5.11 (s, 3H), 2.77–2.73 (m, 2H), 1.30 (t, *J* = 7.6 Hz, 3H). ^{13}C NMR (150 MHz, $CDCl_3$) δ 157.97, 147.69, 146.69, 140.89, 138.83, 132.25, 128.88, 128.70, 128.14, 127.54, 124.70, 119.14, 118.60, 40.79, 28.72, 15.26. HRMS (ESI) *m*/*z* calcd for $C_{24}H_{22}IN$ $[M - I]^+$, 324.1747, found: 324.1756.

*5.2.13.5. (E)-10-methyl-9-(4-butylstyryl)acridin-10-ium iodide. (**15e**).* Brown solid, yield 78%, m.p.: 186–188 °C; ^{1}H NMR (600 MHz, Chloroform-*d*) δ 8.83 (s, 2H), 8.70 (d, *J* = 8.0 Hz, 2H), 8.40 (s, 2H), 8.09 (d, *J* = 15.7 Hz, 1H), 7.89 (s, 2H), 7.69 (d, *J* = 7.7 Hz, 2H), 7.35 (d, *J* = 7.4 Hz, 2H), 7.23 (d, *J* = 15.9 Hz, 1H), 5.14 (s, 3H), 2.73–2.70 (m, 2H), 1.69–1.64 (m, 2H), 1.42–1.39 (m, 2H), 0.97 (t, *J* = 7.4 Hz, 3H). ^{13}C NMR (150 MHz, $CDCl_3$) δ 157.94, 146.71, 146.33, 140.81, 138.79, 132.18, 129.18, 128.86, 128.04, 127.49, 124.63, 119.06, 118.56, 40.73, 35.39, 33.16, 22.06, 13.72. HRMS (ESI) *m*/*z* calcd for $C_{26}H_{26}IN$ $[M - I]^+$, 352.2060, found: 352.2072.

*5.2.13.6. (E)-10-methyl-9-(4-(tert-butyl)styryl)acridin-10-ium iodide. (**15f**).* Brown solid, yield 69%, m.p.: 218–220 °C; ^{1}H NMR (600 MHz, Chloroform-*d*) δ 8.83 (d, *J* = 9.2 Hz, 2H), 8.69 (d, *J* = 8.6 Hz, 2H), 8.41–8.38 (m, 2H), 8.10 (d, *J* = 16.3 Hz, 1H), 7.90–7.87 (m, 2H), 7.73 (d, *J* = 8.3 Hz, 2H), 7.57 (d, *J* = 8.3 Hz, 2H), 7.23 (d, *J* = 16.3 Hz, 1H), 5.13 (s, 3H), 1.40 (s, 9H). ^{13}C NMR (150 MHz, $CDCl_3$) δ 157.96, 154.45, 146.51, 140.81, 138.80, 131.96, 128.85, 127.90, 127.49, 126.08, 124.63, 119.07, 118.78, 40.72, 34.82, 30.93. HRMS (ESI) *m*/*z* calcd for $C_{26}H_{26}IN$ $[M - I]^+$, 352.2060, found: 352.2062.

*5.2.13.7. (E)-10-methyl-9-(4-ethoxystyryl)acridin-10-ium iodide. (**15g**).* Brown solid, yield 67%, m.p.: 186–189 °C; ^{1}H NMR (600 MHz, Chloroform-*d*) δ 8.83 (d, *J* = 9.1 Hz, 2H), 8.69 (d, *J* = 8.6 Hz, 2H), 8.42–8.39 (m, 2H), 8.11 (d, *J* = 16.3 Hz, 1H), 7.92–7.89 (m, 2H), 7.43 (t, *J* = 7.9 Hz, 1H), 7.33 (d, *J* = 7.6 Hz, 1H), 7.29 (s, 1H), 7.18 (d, *J* = 16.3 Hz, 1H), 7.04 (dd, *J* = 8.2, 2.1 Hz, 1H), 5.13 (s, 3H), 4.18–4.14 (m, 2H), 1.48 (t, *J* = 7.0 Hz, 3H). ^{13}C NMR (150 MHz, $CDCl_3$) δ 159.46, 157.75, 146.11, 141.03, 138.95, 136.02, 130.19, 128.94, 127.70, 124.89, 120.47, 119.87, 119.30, 116.94, 113.39, 63.85, 40.94, 14.70. HRMS (ESI) *m*/*z* calcd for $C_{23}H_{20}INO$ $[M - I]^+$, 340.1696, found: 340.1706.

*5.2.13.8. (E)-10-methyl-9-(3,4-dimethoxystyryl)acridin-10-ium iodide. (**15h**).* Brown solid, yield 63%, m.p.: 224–227 °C; ^{1}H NMR (600 MHz, Chloroform-*d*) δ 8.77 (d, *J* = 8.5 Hz, 2H), 8.70 (d, *J* = 9.0 Hz, 2H), 8.36–8.33 (m, 2H), 8.18 (d, *J* = 16.0 Hz, 1H), 7.89–7.86 (m, 2H), 7.41 (s, 1H), 7.33 (d, *J* = 8.1 Hz, 1H), 7.20 (d, *J* = 16.1 Hz, 1H), 6.97 (d, *J* = 8.2 Hz, 1H), 5.02 (s, 3H), 4.06 (s, 3H), 3.98 (s, 3H). ^{13}C NMR (150 MHz, DMSO + $CDCl_3$) δ 157.67, 150.83, 148.70, 147.01, 140.46, 137.55, 128.73, 128.20, 126.74, 123.75, 123.32, 118.57, 118.20, 111.12, 109.89, 55.48, 55.33. HRMS (ESI) *m*/*z* calcd for $C_{24}H_{22}INO_2$ $[M - I]^+$, 356.1645, found: 356.1641.

*5.2.13.9. (E)-10-methyl-9-(2-([1,1′-biphenyl]-4-yl)vinyl)acridin-10-ium iodide. (**15i**).* Dark red solid, yield 71%, m.p.: 209–211 °C; ^{1}H NMR (600 MHz, Chloroform-*d*) δ 8.83 (d, *J* = 9.1 Hz, 2H), 8.73 (d, *J* = 8.5 Hz, 2H), 8.42–8.39 (m, 2H), 8.18 (d, *J* = 16.3 Hz, 1H), 7.91 (dd, *J* = 8.4, 6.9 Hz, 2H), 7.86 (d, *J* = 8.2 Hz, 2H), 7.78 (d, *J* = 8.2 Hz, 2H), 7.68 (d, *J* = 7.1 Hz, 2H), 7.51 (t, *J* = 7.6 Hz, 2H), 7.43 (t, *J* = 7.4 Hz, 1H), 7.28 (d, *J* = 16.4 Hz, 1H), 5.14 (s, 3H). ^{13}C NMR (150 MHz, DMSO) δ 157.20, 145.08, 141.27, 140.44, 138.72, 137.72, 134.27, 128.71, 128.65, 127.63, 126.99, 126.64, 126.31, 123.88, 120.65, 118.67. HRMS (ESI) *m*/*z* calcd for $C_{28}H_{22}IN$ $[M - I]^+$, 372.1747, found: 372.1737.

*5.2.13.10. (E)-10-methyl-9-(4-fluorostyryl)acridin-10-ium iodide. (**15j**).* Brown solid, yield 69%, m.p.: 225–228 °C; ^{1}H NMR (600 MHz, DMSO-d_6) δ 8.86 (d, *J* = 8.6 Hz, 2H), 8.77 (d, *J* = 9.2 Hz, 2H), 8.55 (d, *J* = 16.3 Hz, 1H), 8.45–8.42 (m, 2H), 8.09–8.06 (m, 2H), 8.01–7.99 (m, 2H), 7.40 (t, *J* = 8.6 Hz, 2H), 7.34 (d, *J* = 16.3 Hz, 1H), 4.82 (s, 3H). ^{13}C NMR (150 MHz, DMSO) δ 163.59, 161.94, 157.16, 144.01, 140.47, 137.76, 131.80 (d, $J_{F\text{-}C}$ = 3.2 Hz), 130.31 (d, $J_{F\text{-}C}$ = 8.5 Hz), 128.71, 127.02, 123.89, 120.51 (d, $J_{F\text{-}C}$ = 2.5 Hz), 118.70, 115.55 (d, $J_{F\text{-}C}$ = 21.7 Hz), 48.20. MS (ESI) *m*/*z* calcd for $C_{22}H_{17}FIN$ $[M - I]^+$, 314.13, found: 314.46.

*5.2.13.11. (E)-10-methyl-9-(4-chlorostyryl)acridin-10-ium iodide. (**15k**).* Brown solid, yield 70%, m.p.: 169–172 °C; ^{1}H NMR (600 MHz, Chloroform-*d*) δ 8.84–8.81 (m, 2H), 8.75 (d, *J* = 8.9 Hz, 1H), 8.28 (d, *J* = 8.4 Hz, 2H), 7.96 (d, *J* = 8.2 Hz, 1H), 7.78–7.72 (m,

2H), 7.61 (d, J = 8.3 Hz, 2H), 7.54 (d, J = 8.3 Hz, 2H), 7.28–7.27 (m, 1H), 7.22–7.19 (m, 1H), 5.10 (s, 3H). HRMS (ESI) m/z calcd for $C_{22}H_{17}ClIN$ $[M - I]^+$, 330.1044, found: 330.1046.

*5.2.13.12. (E)-10-methyl-9-(4-bromostyryl)acridin-10-ium iodide. (**15l**).* Brown solid, yield 71%, m.p.: 179–181 °C; ^{1}H NMR (600 MHz, DMSO-d_6) δ 8.84 (d, J = 8.6 Hz, 2H), 8.77 (d, J = 9.2 Hz, 2H), 8.62 (d, J = 16.4 Hz, 1H), 8.45–8.43 (m, 2H), 8.02–7.99 (m, 2H), 7.96 (d, J = 8.4 Hz, 2H), 7.76 (d, J = 8.4 Hz, 2H), 7.31 (d, J = 16.4 Hz, 1H), 4.83 (s, 3H). ^{13}C NMR (150 MHz, DMSO) δ 157.09, 143.72, 140.58, 137.83, 134.43, 131.53, 129.89, 128.77, 127.11, 123.99, 123.18, 121.64, 118.76, 48.21. HRMS (ESI) m/z calcd for $C_{22}H_{17}BrIN$ $[M - I]^+$, 374.0539, found: 374.0542.

*5.2.13.13. (E)-10-methyl-9-(2,4-dichlorostyryl)acridin-10-ium iodide. (**15m**).* Dark red solid, yield 73%, m.p.: 212–215 °C; ^{1}H NMR (600 MHz, DMSO-d_6) δ 8.85–8.84 (m, 2H), 8.79 (d, J = 9.2 Hz, 2H), 8.62 (d, J = 16.3 Hz, 1H), 8.47–8.44 (m, 3H), 8.03–8.00 (m, 2H), 7.82 (d, J = 2.1 Hz, 1H), 7.70 (dd, J = 8.6, 2.1 Hz, 1H), 7.42 (d, J = 16.4 Hz, 1H), 4.85 (s, 3H). ^{13}C NMR (150 MHz, DMSO) δ 156.54, 140.67, 138.30, 137.92, 134.72, 133.85, 131.96, 129.41, 128.98, 128.64, 127.66, 127.24, 124.74, 124.15, 118.84, 48.21. HRMS (ESI) m/z calcd for $C_{22}H_{16}Cl_2IN$ $[M - I]^+$, 364.0654, found: 364.0650.

*5.2.14. 9-(o-Tolylethynyl)acridine (**16b**)*

To a 100 mL round bottom flask containing **7** (0.15 g, 0.58 mmol), was added Pd $(PPh_3)_2Cl_2$ (8.1 mg, 0.01 mmol) and $CuBr_2$ (3.3 mg, 0.02 mmol). Et_3N (10 mL) was added as solvent and the suspension was stirred for 10 min at room temperature under N_2 atmosphere. After 10 min under stirring, phenylacetylene (65 mg, 0.64 mmol) was added and the solution was refluxed at 85 °C for 24 h. When cooled to room temperature, the reaction solution was filtered through Celite. The solvent was removed under reduced pressure and the residue was purified via silica gel using petroleum ether/EtOAc (3/1) as eluent to yield the desired product as a yellow solid (76%, 0.12 g). ^{1}H NMR (400 MHz, Chloroform-d) δ 8.70 (d, J = 8.5 Hz, 2H), 8.29 (d, J = 4.4 Hz, 2H), 7.85–7.81 (m, 2H), 7.75 (dd, J = 7.5, 1.4 Hz, 1H), 7.67–7.63 (m, 2H), 7.48–7.44 (m, 1H), 7.09–7.02 (m, 2H), 4.07 (s, 3H).

*5.2.15. Typical procedure for the synthesis of Series **D***

Compound **17b** (71.6 mg, 68%) were prepared from **16b** (0.1 g, 0.36 mmol) and CH_3I (0.51 g, 3.6 mmol) according to the preparation procedure of **9d** described above.

*5.2.15.1. 10-Methyl-9-(phenylethynyl)acridin-10-ium iodide. (**17a**).* Brown solid, yield 61%, m.p.: 205–209 °C; ^{1}H NMR (600 MHz, DMSO-d_6) δ 9.05 (d, J = 8.5 Hz, 2H), 8.82 (d, J = 9.2 Hz, 2H), 8.49–8.47 (m, 2H), 8.18 (d, J = 7.3 Hz, 2H), 8.14–8.11 (m, 2H), 7.73–7.66 (m, 3H), 4.85 (s, 3H). HRMS (ESI) m/z calcd for $C_{22}H_{16}IN$ $[M - I]^+$, 294.1277, found: 294.1288.

*5.2.15.2. 10-Methyl-9-(o-tolylethynyl)acridin-10-ium iodide. (**17b**).* Brown solid, yield 63%, m.p.: 228–231 °C; ^{1}H NMR (600 MHz, DMSO-d_6) δ 9.05 (d, J = 8.4 Hz, 2H), 8.80 (d, J = 9.2 Hz, 2H), 8.48–8.46 (m, 2H), 8.16–8.14 (m, 2H), 8.08 (d, J = 7.3 Hz, 1H), 7.71 (t, J = 8.2 Hz, 1H), 7.34 (d, J = 8.4 Hz, 1H), 7.21 (t, J = 7.4 Hz, 1H), 4.83 (s, 3H), 4.14 (s, 3H). HRMS (ESI) m/z calcd for $C_{23}H_{18}IN$ $[M - I]^+$, 308.1434, found: 308.1435.

*5.2.15.3. 10-Methyl-9-((2-methoxyphenyl)ethynyl)acridin-10-ium iodide. (**17c**).* Brown solid, yield 59%, m.p.: 218–222 °C; ^{1}H NMR (600 MHz, DMSO-d_6) δ 9.03 (d, J = 8.5 Hz, 2H), 8.79 (d, J = 9.2 Hz, 2H), 8.48–8.45 (m, 2H), 8.16–8.13 (m, 2H), 8.07 (d, J = 7.5 Hz, 1H), 7.72–7.69 (m, 1H), 7.33 (d, J = 8.4 Hz, 1H), 7.20 (t, J = 7.4 Hz, 1H), 4.82 (s, 3H), 4.13 (s, 3H). ^{13}C NMR (150 MHz, DMSO) δ 140.36, 137.77, 134.06, 133.99, 128.47, 127.99, 125.41, 120.54, 118.85, 71.65, 59.63, 55.89, 47.98. HRMS (ESI) m/z calcd for $C_{23}H_{18}INO$ $[M - I]^+$, 324.1383, found: 324.1386.

*5.2.15.4. 10-Methyl-9-(m-tolylethynyl)acridin-10-ium iodide. (**17d**).* Brown solid, yield 62%, m.p.: 203–205 °C; ^{1}H NMR (600 MHz, DMSO-d_6) δ 9.05–9.04 (m, 2H), 8.82 (d, J = 9.2 Hz, 2H), 8.49–8.46 (m, 2H), 8.13–8.11 (m, 2H), 8.02 (s, 1H), 7.98 (d, J = 6.7 Hz, 1H), 7.57–7.53 (m, 2H), 4.85 (s, 3H), 2.46 (s, 3H). HRMS (ESI) m/z calcd for $C_{23}H_{18}IN$ $[M - I]^+$, 308.1434, found: 308.1444.

*5.2.15.5. 10-Methyl-9-((4-ethylphenyl)ethynyl)acridin-10-ium iodide. (**17e**).* Brown solid, yield 66%, m.p.: 182–186 °C; ^{1}H NMR (600 MHz, DMSO-d_6) δ 9.05–9.04 (m, 2H), 8.81 (d, J = 9.2 Hz, 2H), 8.49–8.46 (m, 2H), 8.13–8.10 (m, 4H), 7.52 (d, J = 8.3 Hz, 2H), 4.84 (s, 3H), 2.79–2.75 (m, 2H), 1.26 (t, J = 7.6 Hz, 3H). HRMS (ESI) m/z calcd for $C_{24}H_{20}IN$ $[M - I]^+$, 322.1590, found: 322.1601.

*5.2.15.6. 10-Methyl-9-((4-butylphenyl)ethynyl)acridin-10-ium iodide. (**17f**).* Brown solid, yield 67%, m.p.: 192–194 °C; ^{1}H NMR (600 MHz, DMSO-d_6) δ 9.05–9.03 (m, 2H), 8.80 (d, J = 9.2 Hz, 2H), 8.48–8.45 (m, 2H), 8.12–8.09 (m, 4H), 7.50 (d, J = 8.2 Hz, 2H), 4.84 (s, 3H), 2.75–2.72 (m, 2H), 1.65–1.62 (m, 2H), 1.46–1.44 (m, 2H), 0.95–0.92 (m, 3H). HRMS (ESI) m/z calcd for $C_{26}H_{24}IN$ $[M - I]^+$, 350.1903, found: 350.1906.

*5.2.15.7. 10-Methyl-9-((4-methoxyphenyl)ethynyl)acridin-10-ium iodide. (**17g**).* Brown solid, yield 59%, m.p.: 216–221 °C; ^{1}H NMR (600 MHz, DMSO-d_6) δ 9.03 (d, J = 8.4 Hz, 2H), 8.78 (d, J = 9.1 Hz, 2H), 8.46–8.44 (m, 2H), 8.17 (d, J = 8.6 Hz, 2H), 8.10–8.08 (m, 2H), 7.23 (d, J = 8.6 Hz, 2H), 4.81 (s, 3H), 3.93 (s, 3H). HRMS (ESI) m/z calcd for $C_{23}H_{18}INO$ $[M - I]^+$, 324.1383, found: 324.1384.

*5.2.15.8. 10-Methyl-9-((4-ethoxyphenyl)ethynyl)acridin-10-ium iodide. (**17h**).* Brown solid, yield 65%, m.p.: 179–183 °C; ^{1}H NMR (600 MHz, DMSO-d_6) δ 9.04–9.02 (m, 2H), 8.77 (d, J = 9.2 Hz, 2H), 8.46–8.43 (m, 2H), 8.15 (d, J = 8.8 Hz, 2H), 8.10–8.07 (m, 2H), 7.21 (d, J = 8.8 Hz, 2H), 4.81 (s, 3H), 4.23–4.19 (m, 2H), 1.40 (t, J = 7.0 Hz, 3H). ^{13}C NMR (150 MHz, DMSO) δ 140.26, 137.68, 135.30, 128.73, 127.80, 125.28, 118.73, 114.85, 63.27, 13.85. HRMS (ESI) m/z calcd for $C_{24}H_{20}INO$ $[M - I]^+$, 338.1539, found: 338.1530.

*5.2.15.9. 10-Methyl-9-((4-propoxyphenyl)ethynyl)acridin-10-ium iodide. (**17i**).* Brown solid, yield 63%, m.p.: 194–198 °C; ^{1}H NMR (600 MHz, DMSO-d_6) δ 9.04–9.02 (m, 2H), 8.78 (d, J = 9.2 Hz, 2H), 8.46–8.43 (m, 2H), 8.16 (d, J = 8.8 Hz, 2H), 8.10–8.07 (m, 2H), 7.22 (d, J = 8.8 Hz, 2H), 4.81 (s, 3H), 4.11 (t, J = 6.5 Hz, 2H), 1.82–1.78 (m, 2H), 1.02 (t, J = 7.4 Hz, 3H). HRMS (ESI) m/z calcd for $C_{25}H_{22}INO$ $[M - I]^+$, 352.1696, found: 352.1693.

*5.2.15.10. 10-Methyl-9-([1,1′-biphenyl]-4-ylethynyl)acridin-10-ium iodide. (**17j**).* Brown solid, yield 67%, m.p.: 199–204 °C; ^{1}H NMR (600 MHz, DMSO-d_6) δ 9.10–9.09 (m, 2H), 8.82 (d, J = 9.2 Hz, 2H), 8.50–8.47 (m, 2H), 8.29 (d, J = 8.4 Hz, 2H), 8.14–8.12 (m, 3H), 8.00 (d, J = 8.4 Hz, 2H), 7.86 (d, J = 7.3 Hz, 2H), 7.56 (t, J = 7.6 Hz, 2H), 4.86 (s, 3H). HRMS (ESI) m/z calcd for $C_{28}H_{20}IN$ $[M - I]^+$, 370.1590, found: 370.1574.

5.3. In vitro antibacterial assay

The MIC of the prepared compounds was determined using the standard broth microdilution procedures recommended by CLSI [48,49]. Bacterial strains were incubated on Mueller Hinton Agar (MHA) medium at 37 °C for 24 h and then log-phase bacteria were

suspended in 10 mL sterile water to make a 0.5 McFarland standard inoculum. The standard inoculum was diluted 10 times for further use. A series of gradient solutions of the prepared compounds and the control drugs were prepared in sterile Mueller Hinton (MH) broth by using a 2-fold dilution method with concentrations ranging from 0.125 to 64 μg/mL. Then 5 μL of diluted standard inoculum (1.5×10^7 cfu/mL) was added to the above solutions and 96-well plates were incubated aerobically for 24 h at 37 °C. After 24 h, turbidity was observed and the last tube with no growth of bacteria was recorded to represent the MIC value, expressed in μg/mL.

5.4. Minimum bactericidal concentration (MBC) assay

MBC assay was conducted using the broth microdilution assay described in the preceding section [50]. After 24 h of incubation, 5 μL of the clear solutions from the microtiter wells were plated onto tryptic soy agar (TSA). The TSA plates were incubated aerobically for 24 h at 37 °C. After 24 h, the colonies were observed on TSA plates. If there were no colonies, the corresponding minimum concentration was the MBC value.

5.5. Time-kill curve assay

The log-phase *S. aureus* ATCC 25923 was diluted to approximately 10^6 CFU/mL in volumes of MH broth containing a series of concentrations (1/2, 1, 2 and 4 × MIC) of the test compound. The resultant mixtures were incubated at 37 °C with shaking. 20 μL samples were removed for serial dilution in 180 μL volumes of MH broth at 0, 3, 6, 9, 12 and 24 h, respectively. Then, 10 μL of the above diluted samples were plated onto TSA plates with a smear loop. All TSA plates were incubated at 37 °C for 24 h and the CFU/mL at each time point was obtained by counting colonies. Then, we draw a time-kill curve with data of different concentrations and different time points.

5.6. Biofilm formation quantification assay

Biofilm inhibition was performed using the crystal violet assay as previously described [51]. Bacterial strains were grown overnight in MH medium, washed in fresh media and diluted to an OD_{620} of 0.05. This culture was grown for 5–6 h to mid-log phase (OD_{620} of 0.3–0.5) and then diluted with MH media to an OD_{620} of 0.05. 100 μL of bacterial suspension was aliquoted with certain amounts of the test compounds into the 96-well plate at a final concentration of 64, 32, 16, 8 and 4 μg/mL, set 3 parallel wells for each group. The control group was added to 100 μL of bacterial culture per well and the blank group was added to 100 μL of fresh MH medium. Then the culture was incubated statically for 18 h at 37 °C. After that, the bacterial culture was removed and the 96-well plate washed three times with PBS and dried (pH = 7.2–7.4). The remaining biofilms were fixed with anhydrous methanol for 15 min before dried. Then biofilms were stained with 0.1% (w/v) crystal violet (CV) solution for 30 min. After removing CV, each well was washed three times with distilled water, dried out and solubilized in 120 μL 1% sodium dodecyl sulphate. Biofilm inhibition was determined by measuring the absorbance at 540 nm by a microtiter plate reader. Each assay was performed in triplicate.

5.7. Resistance development study

The propensity of bacterial resistance development for test compound was assessed using a laboratory resistance simulation assay. The initial MIC of the test compound against *S. aureus* ATCC25923 was obtained from the above method. Bacterial cells in a 96-well plate at a concentration of 0.5 × MIC were used to prepare the bacterial suspension (~10^7 CFU/mL) for the next MIC measurement. Ciprofloxacin and rifampicin were used as comparisons to investigate the resistance development. After incubation with sample at 37 °C for 24 h, the new MICs were determined. The experiment process was lasted for 18 passages.

5.8. Visualization of bacterial morphology

The cells of *B. pumilus* CMCC63202 was incubated in MH broth at 37 °C and then the bacterial suspension was diluted with MH broth to an OD_{620} of 0.01. The prepared bacterial solutions contain 0.5 × MIC concentration of the test compound and grow at 37 °C for 18 h. The cells for morphology studies were collected and resuspended in 0.5 mL of PBS buffer and 10 μL of the suspension mixture was transferred on a microscopic slide pretreated with 0.1% (w/v) poly-L-lysine. Phase-contrast light microscope (the Olympus CKX41) was used to capture cell morphology.

5.9. FtsZ polymerization assay

The polymerization of *Bs*FtsZ was monitored using the light scattering assay adapted from the literature [52]. The polymerization was measured using Hitachi fluorescence spectrophotometer (model F-2500) and the excitation and emission wavelengths were set at 411 and 430 nm, respectively. The PMT Voltage was set at 700 V, and the slit width was 5 nm. *Bs*FtsZ (5 μM) in 20 mM of Tris buffer (pH 7.4, containing 20 mM KCl, 5 mM $MgCl_2$ and 0.01% Triton X-100 to avoid compound aggregation) was placed in a fluorometer cuvette, and then was incubated with vehicle (2% DMSO) or different concentrations of the test compound. A final concentration of 2 mM GTP was added at the last fraction and the increase in light scattering was measured for an additional 800s. Moreover, negative control experiments with 10 μg/mL linezolid were performed in the same way.

5.10. Transmission electron microscopy (TEM)

*Bs*FtsZ (5 μM) was incubated in the absence and in the presence of the test compound in polymerization reaction solution described above. After 20 min, 10 μL of the resulting dilutions were placed on glow-discharged Formvar carbon-coated copper grids (400 mesh). After 10 min, the grids were negatively stained with a solution of 1% phosphotungstic acid (PTA) for 1 min and excess PTA was wicked away with filter paper, air-dried. The specimen was then digitally imaged on a transmission electron microscope (HITACHI, HT-7700) interfaced with a CCD camera.

5.11. Hemolytic activity assay

The final concentrations ranged from 1 × MIC to 16 × MIC μg/mL and 50 μL of each was added to 96-well plates. Fresh red blood cells of mice were collected by centrifugation at a speed of 1500 rpm for 10 min. Following that, PBS was used to wash the red blood cells with the same method three times. After addition of 20-fold volume PBS to washed red blood cells, 50 μL of the resulting solution was added to each vial containing the serially diluted compound and incubated at 37 °C for 1 h. 96-well plates were centrifuged at 1500 rpm for 10 min, and then 30 μL of the suspension was taken out and transferred to another 96-well plate containing 70 μL of PBS in each vial. The absorbance of the mixture was observed at 450 nm. The negative control was the PBS buffer not treated with the drug, and the positive control was the PBS buffer treated with 2% Triton. The experiment was performed in triplicate and the hemolysis activity was calculated by the formula %

hemolysis = [(Abs sample − Abs PBS)/(Abs Triton − Abs PBS)] × 100.

5.12. In vivo efficacy

The mid-log phase cultures of *S. aureus* ATCC25923 were centrifuged, and the cell pellets were suspended in sterile saline. These culture suspensions were diluted further in sterile saline to obtain the required CFU of bacteria for infection. All experimental procedures conformed to the animal experiment guidelines of the Animal Care and Welfare Committee of Shandong University. Groups of Kunming mice with an average weight of 25 g were infected intravenously with an inoculum of *S. aureus* ATCC25923 (0.2 mL of saline containing 6×10^7 CFU). About 1 h after infection, the mice were then intraperitoneal administered the test compound dissolved in 0.5 mL vehicle at doses of 1, 5 and 25 mg/kg body weight (6 per group). Linezolid was used as a reference drug in the same manner at the same doses. To evaluate bacteremia, blood samples (100 μL) were obtained from the orbital vein before treatment and 1 h after treatment, and then plated on MH agar using the surface-spread plate method. And then the plates were incubated 24 h for life counting of *S. aureus*.

5.13. Computational study

Molecular docking was performed using Discovery Studio. The X-ray crystal structure of FtsZ (PDB ID: 4DXD; resolution: 2.0 Å) was downloaded from the Protein Data Bank (PDB) database. Water molecules and co-crystal ligands were removed from the structure and the *Sa*FtsZ protein was prepared for further molecular docking. The ligand molecule was built using the Chembio3D software and minimized using the Discovery Studio molecule preparation tools. Through the graphical user interface DS CDocker protocol, automated docking studies were carried out.

Declaration of competing interest

The authors declare that they have no known competing financial interests or personal relationships that could have appeared to influence the work reported in this paper.

Acknowledgements

This work was supported financially by National Natural Science Foundation of China (81973179 and 81673284) and Key Project of Major Project of New and Old Kinetic Energy Conversion of Shandong Province in 2020.

Appendix A. Supplementary data

Supplementary data to this article can be found online at https://doi.org/10.1016/j.ejmech.2021.113480.

References

[1] P.R. Shankar, Book review: tackling drug-resistant infections globally, Arch. Pharm. Pract. 7 (2016) 110.
[2] K. Hardy, P. Hawkey, F. Gao, B. Oppenheim, Methicillin resistant Staphylococcus aureus in the critically ill, Br. J. Anaesth. 92 (2004) 121–130.
[3] I.M. Gould, M.Z. David, S. Esposito, J. Garau, G. Lina, T. Mazzei, G. Peters, New insights into meticillin-resistant Staphylococcus aureus (MRSA) pathogenesis, treatment and resistance, Int. J. Antimicrob. Agents 39 (2012) 96–104.
[4] U. Theuretzbacher, S. Gottwalt, P. Beyer, M. Butler, L. Czaplewski, C. Lienhardt, L. Moja, M. Paul, S. Paulin, J.H. Rex, L.L. Silver, M. Spigelman, G.E. Thwaites, J.P. Paccaud, S. Harbarth, Analysis of the clinical antibacterial and antituberculosis pipeline, Lancet Infect. Dis. 19 (2019) 40–50.
[5] R.L. Lock, E.J. Harry, Cell-division inhibitors: new insights for future antibiotics, Nat. Rev. Drug Discov. 7 (2008) 324–338.
[6] S. Ma, P.S. Ma, The development of FtsZ inhibitors as potential antibacterial agents, ChemMedChem 7 (2012) 1161–1172.
[7] D.W. Adams, J. Errington, Bacterial cell division: assembly, maintenance and disassembly of the Z ring, Nat. Rev. Microbiol. 7 (2009) 642–653.
[8] M. Osawa, D.E. Anderson, H.P. Erickson, Reconstitution of contractile FtsZ rings in liposomes, Science 320 (2008) 792–794.
[9] D. Awasthi, K. Kumar, I. Ojima, Therapeutic potential of FtsZ inhibition: a patent perspective, Expert Opin. Ther. Pat. 21 (2011) 657–679.
[10] P. Domadia, S. Swarup, A. Bhunia, J. Sivaraman, D. Dasgupta, Inhibition of bacterial cell division protein FtsZ by cinnamaldehyde, Biochem. Pharmacol. 74 (2007) 831–840.
[11] R. Jaiswal, T.K. Beuria, R. Mohan, S.K. Mahajan, D. Panda, Totarol inhibits bacterial cytokinesis by perturbing the assembly dynamics of FtsZ, Biochemistry 46 (2007) 4211–4220.
[12] H. Ito, A. Ura, Y. Oyamada, A. Tanitame, H. Yoshida, S. Yamada, M. Wachi, J. Yamagishi, A 4-aminofurazan derivative-A189-inhibits assembly of bacterial cell division protein FtsZ in vitro and in vivo, Microbiol. Immunol. 50 (2006) 759–764.
[13] K. Kumar, D. Awasthi, S.Y. Lee, I. Zanardi, B. Ruzsicska, S. Knudson, P.J. Tonge, R.A. Slayden, I. Ojima, Novel trisubstituted benzimidazoles, targeting Mtb FtsZ, as a new class of antitubercular agents, J. Med. Chem. 54 (2011) 374–381.
[14] D.J. Haydon, J.M. Bennett, D. Brown, I. Collins, G. Galbraith, P. Lancett, R. Macdonald, N.R. Stokes, P.K. Chauhan, J.K. Sutariya, N. Nayal, A. Srivastava, J. Beanland, R. Hall, V. Henstock, C. Noula, C. Rockley, L. Czaplewski, Creating an antibacterial with in vivo efficacy: synthesis and characterization of potent inhibitors of the bacterial cell division protein FtsZ with improved pharmaceutical properties, J. Med. Chem. 53 (2010) 3927–3936.
[15] Y. Ohashi, Y. Chijiiwa, K. Suzuki, K. Takahashi, H. Nanamiya, T. Sato, Y. Hosoya, K. Ochi, F. Kawamura, The lethal effect of a benzamide derivative, 3-methoxybenzamide, can be suppressed by mutations within a cell division gene, ftsZ, in Bacillus subtilis, J. Bacteriol. 181 (1999) 1348–1351.
[16] T.K. Beuria, M.K. Santra, D. Panda, Sanguinarine blocks cytokinesis in bacteria by inhibiting FtsZ assembly and bundling, Biochemistry 44 (2005) 16584–16593.
[17] P.N. Domadia, A. Bhunia, J. Sivaraman, S. Swarup, D. Dasgupta, Berberine targets assembly of Escherichia coli cell division protein FtsZ, Biochemistry 47 (2008) 3225–3234.
[18] M. Lopus, D. Panda, The benzophenanthridine alkaloid sanguinarine perturbs microtubule assembly dynamics through tubulin binding, FEBS J. 273 (2010) 2139–2150.
[19] J.M. Boberek, S. Jem, G. Liam, R. Floyd, Genetic evidence for inhibition of bacterial division protein FtsZ by berberine, PloS One 5 (2010), 13745.
[20] Parhi, Kaul Kelley, D.S. Pilch, E.J. LaVoie, Antibacterial activity of substituted 5-methylbenzo[c]phenanthridinium derivatives, Bioorg. Med. Chem. Lett 23 (2012) 7080–7083.
[21] S.F. Parhi, Kaul Kelley, D.S. Pilch, E.J. LaVoie, Antibacterial activity of substituted dibenzo[a,g]quinolizin-7-ium derivatives, Bioorg. Med. Chem. Lett 22 (2012) 6962–6966.
[22] N. Sun, F.Y. Chan, Y.J. Lu, M.A.C. Neves, H.K. Lui, Y. Wang, K.Y. Chow, K.F. Chan, S.C. Yan, Y.C. Leung, Rational design of berberine-based FtsZ inhibitors with broad-spectrum antibacterial activity, PloS One 9 (2014), 97514.
[23] C. Kelley, Y. Zhang, A. Parhi, M. Kaul, D.S. Pilch, E.J. Lavoie, 3-Phenyl substituted 6,7-dimethoxyisoquinoline derivatives as FtsZ-targeting antibacterial agents, Bioorg. Med. Chem. 20 (2012) 7012–7029.
[24] N. Sun, R.L. Du, Y.Y. Zheng, B.H. Huang, Q. Guo, R.F. Zhang, K.Y. Wong, Y.J. Lu, Antibacterial activity of N-methylbenzofuro[3,2-b]quinoline and N-methylbenzoindolo[3,2-b]-quinoline derivatives and study of their mode of action, Eur. J. Med. Chem. 135 (2017) 1–11.
[25] F. Liu, H. Venter, F. Bi, S.J. Semple, J. Liu, C. Jin, Synthesis and antibacterial activity of 5-methylphenanthridium derivatives as FtsZ inhibitors, Bioorg, Med. Chem. Lett. 27 (2017) 3399–3402.
[26] J. Liu, R. Ma, F. Bi, F. Zhang, C. Hu, H. Venter, Synthesis and antibacterial activity of 5-methylphenanthridium derivatives as FtsZ inhibitors, Bioorg. Med. Chem. Lett 28 (2018) 1825–1831.
[27] A. Sharma, P. Piplani, Design and synthesis of some acridine-piperazine hybrids for the improvement of cognitive dysfunction, Chem. Biol. Drug Des. 90 (2017) 926–935.
[28] D.T. Hogan, T.C. Sutherland, Modern spin on the electrochemical persistence of heteroatom-bridged triphenylmethyl-type radicals, J. Phys. Chem. Lett. (2018) 2825–2829.
[29] L.C. Wilkins, Y. Kim, E.D. Litle, F.P. Gabbaï, Stabilized carbenium ions as latent, Z-type ligands, Angew. Chem. Int. Ed. 58 (2019) 18266–18270.
[30] S. Basili, T.D. Giacco, F. Elisei, R. Germani, An acridinium-based sensor as a fluorescent photoinduced electron transfer probe for proton detection modulated by anionic micelles, Org. Biomol. Chem. 12 (2014) 6677–6683.
[31] M. Kishimoto, K. Kondo, M. Akita, M. Yoshizawa, A pH-responsive molecular capsule with an acridine shell: catch and release of large hydrophobic compounds, Chem. Commun. 53 (2017) 1425–1428.
[32] A. Jana, B. Saha, D.R. Banerjee, S.K. Ghosh, K.T. Nguyen, X. Ma, Q. Qu, Y. Zhao, N.D.P. Singh, Photocontrolled nuclear-targeted drug delivery by single component photoresponsive fluorescent organic nanoparticles of acridin-9-methanol, Bioconjugate Chem. 24 (2013) 1828–1839.
[33] M. Bečka, M. Vilková, O. Salem, J. Kaščárková, V. Brabec, M. Kožurková, 3-[(E)-(acridin-9′-ylmethylidene)amino]-1-substituted thioureas and their biological activity, Spectroc. Acta Pt. A-Molec. Biomolec. Spectr. 180 (2017) 234–241.

[34] V. Fasano, L.D. Curless, J.E. Radcliffe, M.J. Ingleson, Frustrated lewis pair mediated 1,2-hydrocarbation of alkynes, Angew. Chem. Int. Ed. 56 (2017) 9202–9206.
[35] Y.N. Wang, R.R.Y. Bheemanaboina, W.W. Gao, J. Kang, G.X. Cai, C.H. Zhou, Discovery of benzimidazole–quinolone hybrids as new cleaving agents toward drug-resistant Pseudomonas aeruginosa DNA, ChemMedChem 13 (2018) 1004–1017.
[36] K. Jiang, X. Yan, J. Yu, Z. Xiao, F. Lin, Design, synthesis, and biological evaluation of 3-amino-2-oxazolidinone derivatives as potent quorum-sensing inhibitors of Pseudomonas aeruginosa PAO1, Eur. J. Med. Chem. 194 (2020), 112252.
[37] W. Chin, G. Zhong, Q. Pu, C. Yang, W. Lou, P.F.D. Sessions, B. Periaswamy, A. Lee, Z.C. Liang, X. Ding, A macromolecular approach to eradicate multidrug resistant bacterial infections while mitigating drug resistance onset, Nat. Commun. 9 (2018) 1–14.
[38] P. Vikesland, E. Garner, S. Gupta, S. Kang, A. Maile-Moskowitz, N. Zhu, Differential drivers of antimicrobial resistance across the world, Accounts Chem. Res. 52 (2019) 916–924.
[39] B. Li, S. Ni, F. Mao, F. Chen, Y. Liu, H. Wei, W. Chen, J. Zhu, L. Lan, J. Li, Novel terminal bipheny-based diapophytoene desaturases (CrtN) inhibitors as anti-MRSA/VISR/LRSA agents with reduced hERG activity, J. Med. Chem. 61 (2018) 224–250.
[40] M. Kieron, G. O'Connell, T. James, F. Hodgkinson Hannah, Sore, combating multidrug-resistant bacteria: current strategies for the discovery of novel antibacterials, Angew. Chem. Int. Ed. 52 (2013) 10706–10733.
[41] D.J. Haydon, N.R. Stokes, R. Ure, G. Galbraith, J.M. Bennett, D.R. Brown, P.J. Baker, V.V. Barynin, D.W. Rice, S.E. Sedelnikova, An inhibitor of FtsZ with potent and selective anti-staphylococcal activity, Science 321 (2008) 1673–1675.
[42] S. Ma, C. Cong, X. Meng, S. Cao, H. Yang, Y. Guo, X. Lu, S. Ma, Synthesis and on-target antibacterial activity of novel 3-elongated arylalkoxybenzamide derivatives as inhibitors of the bacterial cell division protein FtsZ, Bioorg. Med. Chem. Lett 23 (2013) 4076–4079.
[43] D.W. Adams, W.L. Juan, L.G. Czaplewski, E. Jeff, Multiple effects of benzamide antibiotics on FtsZ function, Mol. Microbiol. 80 (2011) 68–84.
[44] J.M. Andreu, S.B. Claudia, H. Sonia, A. Dulce, M.L. Lopez-Rodriguez, L.B. Ruiz-Avila, N.E.R. Rafael, L. Oscar, A.J. Martín-Galiano, The antibacterial cell division inhibitor PC190723 is an FtsZ polymer-stabilizing agent that induces filament assembly and condensation, J. Biol. Chem. 285 (2010) 14239–14246.
[45] S. Ning, F.Y. Chan, Y.J. Lu, M. Neves, H.K. Lui, Y. Wang, K.Y. Chow, K.F. Chan, S.C. Yan, Y.C. Leung, Rational design of berberine-based FtsZ inhibitors with broad-spectrum antibacterial activity, PloS One 9 (2014), 97514.
[46] P.B. Noto, G. Abbadessa, M. Cassone, G.D. Mateo, A. Agelan, J.D. Wade, Alternative stabilities of a proline-rich antibacterial peptide in vitro and in vivo, Protein Sci. 17 (2008) 1249–1255.
[47] Q. Zhang, Y. Xu, Q. Wan, B. Hang, Y. Sun, X. Wei, Potential of novel antimicrobial peptide P3 from bovine erythrocytes and its analogs to disrupt bacterial membranes in vitro and display activity against drug-resistant bacteria in a mouse model, Antimicrob. Agents Chemother. 59 (2015) 2835–2841.
[48] F.R. Cockerill, M.A. Wiker, J. Alder, M.N. Dudley, G.M. Eliopoulos, M.J. Ferraro, D.J. Hardy, D.W. Hecht, J.A. Hindler, J.B. Patel, Methods for Dilution Antimicrobial Susceptibility Tests for Bacteria that Grow Aerobically ; Approved Standard — Ninth Edition, Clinical & Laboratory Standards Institute, 2012.
[49] Y. Qin, Y. Teng, R. Ma, F. Bi, Z. Liu, P. Zhang, S. Ma, Design, synthesis and antibacterial evaluation of novel 15-membered 11a-azahomoclarithromycin derivatives with the 1, 2, 3-triazole side chain, Eur. J. Med. Chem. 180 (2019) 321–339.
[50] Y. Qin, S. Qiang, S. Ji, Z. Liu, C. Hu, S. Ma, Synthesis and antibacterial activity of novel 3-O-arylalkylcarbamoyl-3-O-descladinosyl-9-O-(2-chlorobenzyl)oxime clarithromycin derivatives, Bioorg. Med. Chem. Lett 28 (2018) 3324–3328.
[51] G. Brackman, M. Risseeuw, S. Celen, P. Cos, L. Maes, H.J. Nelis, S.V. Calenbergh, T. Coenye, Synthesis and evaluation of the quorum sensing inhibitory effect of substituted triazolyldihydrofuranones, Bioorg. Med. Chem. 20 (2012) 4737–4743.
[52] T.K. Beuria, S.S. Krishnakumar, S. Sahar, N. Singh, K. Gupta, M. Meshram, D. Panda, Glutamate-induced assembly of bacterial cell division protein FtsZ*, J. Biol. Chem. 278 (2003) 3735–3741.